



**DESIGNING OF CRASH BOX AND BUMPER
SYSTEM IN TERMS OF STRENGTH/WEIGHT
RATIO**

**2024
MASTER THESIS
MECHANICAL ENGINEERING**

Gökhan KAYA

**Thesis Advisors
Assoc. Prof. Dr. Mehmet Erdi KORKMAZ
Assoc. Prof. Dr. Munish Kumar GUPTA**

**DESIGNING OF CRASH BOX AND BUMPER SYSTEM IN TERMS OF
STRENGTH/WEIGHT RATIO**

Gökhan KAYA

Thesis Advisors

Assoc. Prof. Dr. Mehmet Erdi KORKMAZ

Assoc. Prof. Dr. Munish Kumar GUPTA

T.C.

Karabük University

Institute of Graduate Programs

Department of Mechanical Engineering

Prepared as

Master Thesis

KARABUK

January 2024

I certify that in my opinion the thesis submitted by Gökhan KAYA titled “DESIGNING OF CRASH BOX AND BUMPER SYSTEM IN TERMS OF STRENGTH/WEIGHT RATIO” is fully adequate in scope and in quality as a thesis for the degree of Master of Science.

Assoc. Prof. Dr. Mehmet Erdi KORKMAZ
Thesis Advisor, Department of Mechanical Engineering

Assoc. Prof. Dr. Munish Kumar GUPTA
Thesis Co-Advisor, Department of Mechanical Engineering

This thesis is accepted by the examining committee with a unanimous vote in the Department of Mechanical Engineering as a Master of Science thesis. January 05, 2024

Examining Committee Members (Institutions) Signature

Chairman : Prof. Dr. Mustafa GÜNAY (KBU)

Member : Assoc. Prof. Dr. Mehmet Erdi KORKMAZ (KBU)

Member : Assoc. Prof. Dr. Munish Kumar GUPTA (PO)

Member : Assoc. Prof. Dr. Recep DEMİRSÖZ (KBU)

Member : Assoc. Prof. Dr. Nafiz YAŞAR (KDU)

The degree of Master of Science by the thesis submitted is approved by the Administrative Board of the Institute of Graduate Programs, Karabuk University.

Assoc. Prof. Dr. Zeynep ÖZCAN
Director of the Institute of Graduate Programs

“I declare that all the information within this thesis has been gathered and presented in accordance with academic regulations and ethical principles and I have according to the requirements of these regulations and principles cited all those which do not originate in this work as well.”

Gökhan KAYA

It is dedicated to our martyrs...

ABSTRACT

M. Sc. Thesis

DESIGNING OF CRASH BOX AND BUMPER SYSTEM IN TERMS OF STRENGTH/WEIGHT RATIO

Gökhan KAYA

Karabük University

Institute of Graduate Programs

The Department of Mechanical Engineering

Thesis Advisors:

Assoc. Prof. Dr. Mehmet Erdi KORKMAZ

Assoc. Prof. Dr. Munish Kumar GUPTA

January 2024, 88 pages

Traffic accidents are an inevitable fact of our daily lives. Approximately 1.3 million people lose their lives each year due to traffic accidents. Millions of people are injured due to traffic accidents, and many of them live disabled as a result of these injuries. Although traffic accidents are not always fatal, they also cause material damage. Scientific studies are extremely important to reduce deaths and injuries as a result of traffic accidents and to enable people to live their lives healthily, as well as to reduce traffic accidents with material damage. Crash boxes and bumper systems play a vital role in preventing deaths and injuries and reducing material damage in traffic accidents. This master thesis named “Designing crash box and bumper system in terms of strength/weight ratio” aims to create a lightweight and robust front crash system (FCS) consisting of the crash box and bumpers. In this study, the front bumper and crash boxes of the vehicle were subjected to crash tests under dynamic loads. The crash

system is made out of aluminum 6000 series. The cross-sections of the crash boxes and certain regions of the front bumper were topologically optimized according to their crashworthiness and energy absorption capabilities. Finally, the studies carried out are summarized in the conclusion part. The boundary conditions of the crash tests were taken from The European New Car Assessment Programme (Euro NCAP).

Keywords: Crash box, bumper system, crashworthiness, energy absorption, topology optimization, crashworthiness optimization, structural optimization.

Science Code: 91406

ÖZET

Yüksek Lisans Tezi

ÇARPIŞMA KUTUSU VE TAMPONLARIN DAYANIM/AĞIRLIK ORANINA GÖRE TASARIMI

Gökhan KAYA

Karabük Üniversitesi

Lisansüstü Eğitim Enstitüsü

Makine Mühendisliği Anabilim Dalı

Tez Danışmanları:

Doç. Dr. Mehmet Erdi KORKMAZ

Doç. Dr. Munish Kumar GUPTA

Ocak 2024, 88 sayfa

Trafik kazaları günlük hayatımızın kaçınılmaz bir gerçeğidir. Trafik kazaları nedeniyle her yıl yaklaşık 1,3 milyon kişi hayatını kaybediyor. Milyonlarca insan trafik kazaları nedeniyle yaralanmakta ve pek çoğu bu yaralanmalar sonucunda yaşamlarını engelli olarak sürdürmektedir. Trafik kazaları her zaman ölümcül olmasa da maddi hasara da neden olmaktadır. Trafik kazaları sonucu ölüm ve yaralanmaların azaltılması ve insanların hayatlarını sağlıklı bir şekilde sürdürebilmeleri, ayrıca maddi hasarlı trafik kazalarını azaltmak için için bilimsel çalışmalar son derece önemlidir. Çarpışma kutusu ve tampon sistemleri trafik kazalarında ölüm ve yaralanmaların önlenmesinde ve maddi hasarın azaltılmasında hayati rol oynamaktadır. “Çarpışma kutusu ve tampon sisteminin mukavemet/ağırlık oranına göre tasarlanması” başlıklı bu yüksek lisans tezi, çarpışma kutusu ve tamponlardan oluşan hafif ve sağlam bir ön çarpışma sistemi (CS) oluşturmayı amaçlamaktadır. Bu çalışmada aracın ön tamponu ve çarpışma

kutuları dinamik yükler altında çarpışma testlerine tabi tutulmuştur. Malzeme olarak alüminyum 6000 serisi kullanılmıştır. Çarpışma kutularının kesitleri ve ön tamponun belirli bölgeleri, çarpma dayanıklılığı ve enerji emme yeteneklerine göre topolojik olarak optimize edildi. Son olarak sonuç kısmında yapılan çalışmalar özetlenmiştir. Çarpışma testlerinin sınır koşulları Avrupa Yeni Araç Değerlendirme Programından (Euro NCAP) alınmıştır.

Anahtar Kelimeler: Çarpışma kutusu, tampon sistemi, çarpışmaya dayanıklılık, enerji emilimi, topoloji optimizasyonu, çarpışmaya dayanıklılık optimizasyonu, yapısal optimizasyon.

Bilim Kodu: 91406

ACKNOWLEDGMENT

Initially, it is my pleasure to express my gratitude to my project advisor, Assoc. Prof. Dr. Mehmet Erdi KORKMAZ and Assoc. Prof. Dr. Munish Kumar GUPTA, for granting me this chance to go through enriching my thesis. Without their cooperation, this thesis would not have been probable. I take this opportunity to show gratitude to my advisor for his valuable guidance and suggestions throughout this thesis.

I additionally want to show gratitude to my dear family for supporting me during my entire master's program.

I would also like to thank my dear sister Emriye KAYA, who has always supported me throughout my life. I would never have come to this day without her support.

CONTENTS

	<u>Page</u>
APPROVAL.....	ii
ABSTRACT.....	v
ÖZET.....	vii
ACKNOWLEDGMENT.....	ix
CONTENTS.....	x
LIST OF FIGURES	xiv
LIST OF TABLES	xviii
SYMBOLS AND ABBREVIATIONS INDEX	xx
PART 1.....	2
INTRODUCTION	2
1.1. PROBLEM STATEMENT	2
1.2. RESEARCH OBJECTIVES AND SIGNIFICANCE	2
1.2.1. Lightweight Structure	2
1.2.2. Design Parameters	4
1.2.3. Improved Safety.....	6
1.2.4. Reduced CO2 Emissions	6
1.3. RESEARCH QUESTIONS	7
1.4. LIMITATIONS	7
1.5. RESEARCH PURPOSE.....	7
1.6. TYPES OF CRASH TESTS.....	7
1.6.1. Frontal Collision	8
1.6.1.1. Full Width Frontal Collision (FWFC)	8
1.6.1.2. Offset Frontal Collision (OFC).....	9
1.6.2. Lateral Collision (LC).....	10
1.6.3. Roll Over Collision.....	11
PART 2.....	12

	<u>Page</u>
LITERATURE REVIEW.....	12
PART 3.....	37
THEORETICAL BACKGROUND.....	37
3.1. FINITE ELEMENT METHOD.....	37
3.1.1. What is finite element method?	37
3.2.2. Governing equations of FEM's	38
3.2 SIMULIA ABAQUS/CAE.....	38
3.2.1. Simulation Steps	38
3.2.1.1. Pre-Processing.....	39
3.2.1.2. Solver	40
3.2.1.3 Post-processing	41
3.3. ABAQUS/EXPLICIT.....	41
3.3.1. Structural Crashworthiness.....	41
3.3.2. Drop Test	42
3.3.3. Passenger Safety	42
3.4. CRASH BOX THEORETICAL FORMULAS	42
3.4.1. Energy Absorption (EA).....	43
3.4.2. Specific Energy Absorption (SEA)	43
3.4.3. Mean Crashing Force (Favg)	43
3.4.4. Crash force efficiency (CFE).....	43
3.5. UNITS	44
3.6. MATERIAL	44
3.6.1. Importance of Aluminum Alloy AA6061-T4.....	44
3.6.1.1. Chemical components of aluminum alloy AA6061-T4.....	44
3.6.2. Properties of AA6061-T4	45
3.6.2.1. Mechanical properties of AA6061-T4	45
3.6.2.2. Physical properties of AA6061-T4	46
3.6.2.3. Thermal properties of AA6061-T4	46
PART 4.....	47
CRASH TESTS AND COMPARISON WITH FEM	47

	<u>Page</u>
THIN-WALLED CRASH TUBES	47
4.1. SINGLE CELL CRASH TUBES	47
4.1.1. Single-cell rectangular tube (SCR)	47
4.1.1.1. Simulation conditions of SCR	48
4.1.1.2. Dynamic simulation results of the SCR	48
4.1.2. Single-cell circular tube (SCC)	50
4.1.2.1 Simulation conditions of SCC	50
4.1.2.2. Dynamic simulation results of the SCC	51
4.1.3. Single-cell hexagonal tube (SCH)	53
4.1.3.1. Simulation conditions of SCH	53
4.1.3.2. Dynamic simulation results of the SCH	55
4.2. MULTI-CELL CRASH TUBES	56
4.2.1. Multi-cell rectangular tube (MCR)	56
4.2.1.1. Simulation conditions of MCR	56
4.2.1.2. Dynamic simulation results of the MCR	58
4.2.2. Multi-cell circular tube (MCC)	59
4.2.2.1. Simulation conditions of MCC	61
4.2.2.2. Dynamic simulation results of the MCC	62
4.3.1. Multi-cell hexagonal tube (MCH)	63
4.3.1.1. Simulation conditions of MCH	63
4.3.1.2. Dynamic simulation results of the MCH	64
4.3. SINGLE-CELL BUMPER BEAM (SCB)	66
4.3.1. Simulation conditions of SCB	66
4.3.2. Dynamic simulation results of the SCB	67
4.4. MULTI-CELL BUMPER BEAM (MCB)	69
4.3.1. Simulation conditions of MCB	69
4.3.2. Dynamic simulation results of the MCB	70
 PART 5	 73
RESULTS AND DISCUSSION	73
5.1. WEIGHT COMPARISON	76
5.2. ENERGY ABSORPTION COMPARISON	77

	<u>Page</u>
5.3. MAXIMUM IMPACT FORCE	77
5.4. SPECIFIC ENERGY ABSORPTION.....	78
PART 6.....	79
CONCLUSION.....	79
REFERENCES.....	80
RESUME.....	88

LIST OF FIGURES

	<u>Page</u>
Figure 1.1. The crash box tubes located between the chassis and the bumper beams are shown in red.	1
Figure 1.2. Bumper beams are shown in red.....	1
Figure 1.3. Crash boxes and front bumper beams are shown together on the car in red.	2
Figure 1.4. Steels used in the Volvo XC40 model [2].	3
Figure 1.5. Circular cross-sectional crash tube with groove stamp.	5
Figure 1.6. Rectangular cross-sectional tapered crash tube with double groove stamp.	5
Figure 1.7. Rectangular cross-sectional tapered crash tube	6
Figure 1.8. Frontal collision test of Chevrolet Camaro.....	8
Figure 1.9. Full width collision of a vehicle tested by Euro NCAP with a rigid wall.	9
Figure 1.10. Offset frontal collision of a vehicle tested by Euro NCAP with a rigid wall.....	9
Figure 1.11. Lateral collision test between test car and deformable barrier.	10
Figure 1.12. Lateral collision test between test car and rigid pole.....	11
Figure 1.13. Roll over collision of the test car.....	11
Figure 2.1. Crash box tubes and bumper beams shown in red.....	12
Figure 2.2. Specimens used in the tests [16].....	13
Figure 2.3. The traditional front bumper system of a car [17].....	14
Figure 2.4. Hexagonal cells and parameters of NPR structure [17].....	15
Figure 2.5. The initial rigid bumper beam (left) and the NPR bumper beam are revealed. (right) [17].	15
Figure 2.6. Deformation of NSGA-II optimized bumper (left) and ESA optimized bumper beam. (right) [17].	16
Figure 2.7. Energy absorption methods [20].....	16
Figure 2.8. MSSQ (A), CSQ (B) and CSTQ (C) structures [20].	17
Figure 2.9. Representation of the MPR structure (left) and foam-filled double tube (right) [21].....	18

	<u>Page</u>
Figure 2.10. Mono-tubular (left), bi-tubular (middle), and tri-tubular axial foam-filled circular tubes with different foam heights [22].	18
Figure 2.11. Deformation of lateral foam-filling circular tubes [22].	19
Figure 2.12. Koch fractal (KF)(green) structures illustration [23].	20
Figure 2.13. Circular Koch fractal (C-KF) (blue) structures illustration [23].	20
Figure 2.14. Hybrid Koch fractal (H-KF) (brown) structures illustration [23].	20
Figure 2.15. Specimens used by LI, Zhixiang [24].	21
Figure 2.16. FEA model of CCST [24].	21
Figure 2.17. Front attenuator model of Formula SAE car [9].	23
Figure 2.18. Microstructure images of XPS-400 left and EPP-5130 right [30].	24
Figure 2.19. Energy/mass and displacement table of materials used in the tests [31].	25
Figure 2.20. Cross-sections of single/double-walled (SW/DW) tubes [32].	25
Figure 2.21. Single/double-walled (SWFF/DWFF) foam-filled tubes [32].	26
Figure 2.22. Deformation shapes of SW [32].	26
Figure 2.23. Deformation shapes of DW [32].	26
Figure 2.24. Deformation shapes of SWFF [32].	27
Figure 2.25. Deformation shapes of DWFF tubes [32].	27
Figure 2.26. Assembly of the front crash system with mass blocks [34].	28
Figure 2.27. The variables to be optimized [34].	28
Figure 2.28. Optimal bumper beam cross-sections (left) and the original ones. (right) [34].	29
Figure 2.29. FEA model representation and multi-cell geometries' cross-sections used by Tran [35].	29
Figure 3.1. FEM representation of a car tested by Euro NCAP.	37
Figure 3.2. Physical appearance of the mechanical part to be simulated in the pre-processing stage.	39
Figure 3.3. FEM appearance of the mechanical part to be simulated in the pre-processing stage.	40
Figure 3.4. Stress distribution of the simulated part under loading.	40
Figure 3.5. Original image and deformed image of the simulated part in the pre-processing stage.	41
Figure 3.6. Abaqus/Explicit crash simulation of a car.	42
Figure 4.1. Rectangular cross-section crash box.	47
Figure 4.2. SCR and rigid wall representation.	48
Figure 4.3. Folding process of SCR.	49

	<u>Page</u>
Figure 4.4. Absorbed energy during the crash of SCR.	49
Figure 4.5. Von misses (left) and displacement (right) of SCR.....	50
Figure 4.6. Circular cross-section crash box representation.	51
Figure 4.7. Folding process of SCC.....	52
Figure 4.8. Absorbed energy during the crash of SCC.	52
Figure 4.9. Von misses (left) and displacement (right) of SCC.....	53
Figure 4.10. Hexagonal cross-section crash box representation.	54
Figure 4.11. Folding process of SCH.....	55
Figure 4.12. Absorbed energy during the crash of SCH.	55
Figure 4.13. Von misses (left) and displacement (right) of SCH.	56
Figure 4.14. Rectangular multi-cell cross-section crash box.	57
Figure 4.15. Transparent and FEM representation of MCR.	57
Figure 4.16. Folding process of MCR.....	58
Figure 4.17. Absorbed energy during the crash of MCR.....	58
Figure 4.18. Von misses (left) and displacement (right) of MCR.	59
Figure 4.19. MCC representation.....	60
Figure 4.20. Sectioned view of MCC at time 0.....	60
Figure 4.21. Sectioned view of MCC at first fold.....	60
Figure 4.22. Sectioned view of MCC at second fold.	61
Figure 4.23. Sectioned view of MCC at the final.	61
Figure 4.24. Absorbed energy during the crash of MCC.....	62
Figure 4.25. MCH representation.....	63
Figure 4.26. Folding process of the MCH.	64
Figure 4.27. Axial folding process representation of the MCH.....	64
Figure 4.28. Von misses (left) and displacement (right) of MCH.	65
Figure 4.29. Sandwich composite structure [76].	65
Figure 4.30. SCB representation.	66
Figure 4.31. SCB initial representation.....	67
Figure 4.32. SCB crash representation at time 0.025 ms.	67
Figure 4.33. SCB crash representation at time 0.05 ms.	68
Figure 4.34. SCB crash box and beam representation at time 0.05 ms.....	68
Figure 4.35. Absorbed energy of SCB.	68
Figure 4.36. MCB representation.....	69

	<u>Page</u>
Figure 4.37. MCB initial representation	70
Figure 4.38. MCB crash representation at time 0.025 ms.....	70
Figure 4.39. MCB crash representation at time 0.05 ms.....	71
Figure 4.40. MCB crash box and beam representation at time 0.05 ms.	71
Figure 4.41. Absorbed energy of MCB.....	71
Figure 4.42. Von Misses (left) and displacement (right) values of MCB.....	72

LIST OF TABLES

	<u>Page</u>
Table 1.1. Fuel consumption and CO ₂ emission comparison [1].....	2
Table 1.2. Percentage of materials used in a car.....	4
Table 2.1. Experimental results of tests [16].	14
Table 2.2. Representation of Koch structure curves with orders [23].	19
Table 2.3. Mass comparison of the structures [31].	25
Table 2.4. Optimal values for three types of crash tubes in terms of Specific Energy Absorption (SEA) and Peak Crashing force (PCF).....	30
Table 2.5. Other studies related to this thesis subject.	31
Table 3.1. Governing equations of physical simulations [54].	38
Table 3.2. Units of Abaqus software.....	44
Table 3.3. Chemical components percentage in weight of AA6061-T4.....	45
Table 3.4. Mechanical properties of AA6061-T4.	45
Table 3.5. Physical properties of AA6061-T4.	46
Table 3.6. Thermal properties of AA6061-T4.	46
Table 4.1. Simulation conditions of SCR.	48
Table 4.2. Simulation results of SCR.....	50
Table 4.3. Simulation conditions of SCC.	51
Table 4.4. Simulation results of SCC.....	53
Table 4.5. Simulation conditions of SCH.	54
Table 4.6. Simulation results of SCH.....	56
Table 4.7. Simulation conditions of MCR.	57
Table 4.8. Simulation results of MCR.	59
Table 4.9. Simulation conditions of MCC.	61
Table 4.10. Simulation results of MCC.	62
Table 4.11. Simulation conditions of MCH.....	63
Table 4.12. Simulation results of MCH.	64
Table 4.13. Simulation conditions of SCB.	66
Table 4.14. Simulation results of SCB.....	67
Table 4.15. Simulation conditions of MCB.	69
Table 4.16. Simulation results of MCB.	70

	<u>Page</u>
Table 5.1. Crash Box tubes and bumper beams representations.....	73
Table 5.2. Simulation Results-I.....	74
Table 5.3. Simulation Results-II.	75
Table 5.4. Mass comparison of tubes.....	76
Table 5.5. Energy absorption comparison of tubes.....	77
Table 5.6. Fmax comparison of tubes.	78
Table 5.7. SEA comparison of tubes.....	78

SYMBOLS AND ABBREVIATIONS INDEX

SYMBOLS

F_{max} : Maximum initial force

F_{avg} : Mean load

f_t : Frictional force

V : Volume loss

L : Length

N : Newton

mm : Millimeter

μm : Micro-meter

m : Meter

k : Friction coefficient

K : Global stiffness matrix

u : Nodal displacement

F : Nodal force

ABBREVIATIONS

<i>FCS</i>	: Front crash system
<i>FEA</i>	: Finite element analysis
<i>Euro NCAP</i>	: European New Car Assessment Programme
<i>BIW</i>	: Body in white
<i>WHO</i>	: World health organization
<i>ZEV</i>	: Zero emission vehicle
<i>CAE</i>	: Computer aided engineering
<i>FWFC</i>	: Full width frontal collision
<i>OFC</i>	: Offset frontal collision
<i>LC</i>	: Lateral collision
<i>ROC</i>	: Roll over collision
<i>MSSQ</i>	: Multi-stage square tube
<i>CSQ</i>	: Conventional square tube
<i>CTSQ</i>	: Conventional tri-tubular tube
<i>S</i>	: Simple tube
<i>SWCD</i>	: Corrugated tube
<i>CWCD</i>	: Composite covered corrugated tube
<i>NPR</i>	: Negative poisson's ratio
<i>PPR</i>	: Positive poisson's ratio
<i>MPR</i>	: Mixed poisson's ratio
<i>SEA</i>	: Specific energy absorption
<i>CFE</i>	: Crash force efficiency
<i>KF</i>	: Koch fractal
<i>C-KF</i>	: Circular Koch fractal
<i>H-KF</i>	: Hybrid Koch fractal
<i>AA</i>	: Aluminum alloy
<i>CCST</i>	: Circumferentially corrugated square tube
<i>MCF</i>	: Mean crashing force
<i>CFRP</i>	: Carbon-fiber reinforced plastic
<i>XPP</i>	: Extruded polystyrene
<i>EPP</i>	: Expanded polystyrene

<i>SW</i>	: Single-walled
<i>DW</i>	: Double-walled
<i>SWFF</i>	: Single-walled foam filled
<i>DWFF</i>	: Double-walled foam filled
<i>PCF</i>	: Peak crashing force
<i>C2C</i>	: Connect to connect
<i>W2W</i>	: Web to web
<i>HCT</i>	: Hybrid corrugated tube
<i>OCT</i>	: Ordinary corrugated tube
<i>SCR</i>	: Single-cell rectangular
<i>SCC</i>	: Single-cell circular
<i>SCH</i>	: Single-cell hexagonal
<i>MCR</i>	: Multi-cell ractangular
<i>MCC</i>	: Multi-cell circular
<i>MCH</i>	: Multi-cell hexagonal
<i>SCB</i>	: Single-cell beam
<i>MCB</i>	: Multi-cell beam

PART 1

INTRODUCTION

Today, transportation and mobility vehicles are increasing rapidly. This rapid increase comes with some problems such as vehicle and passenger safety and environmental pollution. Vehicle companies must fulfill certain regulations to protect passengers from fatal injuries and deaths in the event of an accident. With the desire to gain the trust of customers by producing the safest vehicle and the development of production technology, companies increased their investments in vehicle safety and passenger safety. The use of aluminum and its alloys, which are lighter than heavy materials such as steel, has increased crashworthiness as well. Using these lightweight materials has decreased the total weight of a car. With a 10% reduction in vehicle weight by using lightweight materials, fuel consumption was reduced by 6% to 8% [1]. CO₂ emissions have decreased dramatically as well. Thus, with the use of light metals, the effect on environmental pollution has decreased.

Table 1.1. Fuel consumption and CO₂ emission comparison [1].

	All steel body	All aluminum body
Total vehicle weight	2500kg	2075kg
Average fuel consumption	11.8L/100km	9.9L/100km
Average CO ₂ emission	220g/km	199g/km

1.1. PROBLEM STATEMENT

If the kinetic energy released during an accident is not absorbed, it causes serious damage to the vehicle and the passenger. The FCS consisting of crash box tubes and front bumper beams is a system that absorbs the kinetic energy generated in the event of an accident and is of vital importance. The driver and passenger must be in a safe environment at the time of the accident. The goal here is to improve the current FCS

system and maintain a safe environment. Another goal is to develop a lightweight, robust and low-cost FCS from an engineering perspective.

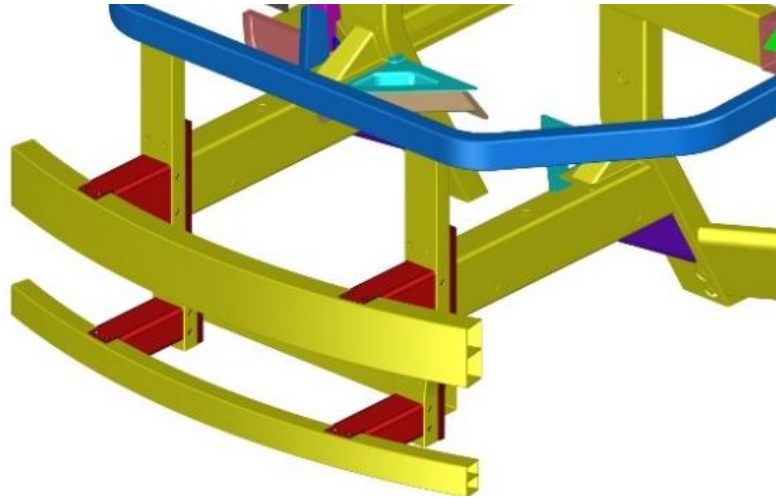


Figure 1.1. The crash box tubes located between the chassis and the bumper beams are shown in red.

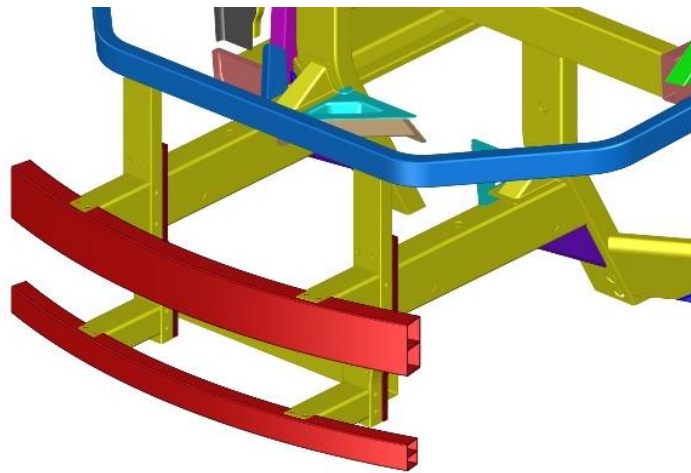


Figure 1.2. Bumper beams are shown in red.

Some companies double the number of tubes and beams in the commercial and hatchback vehicles they produce for safer driving.

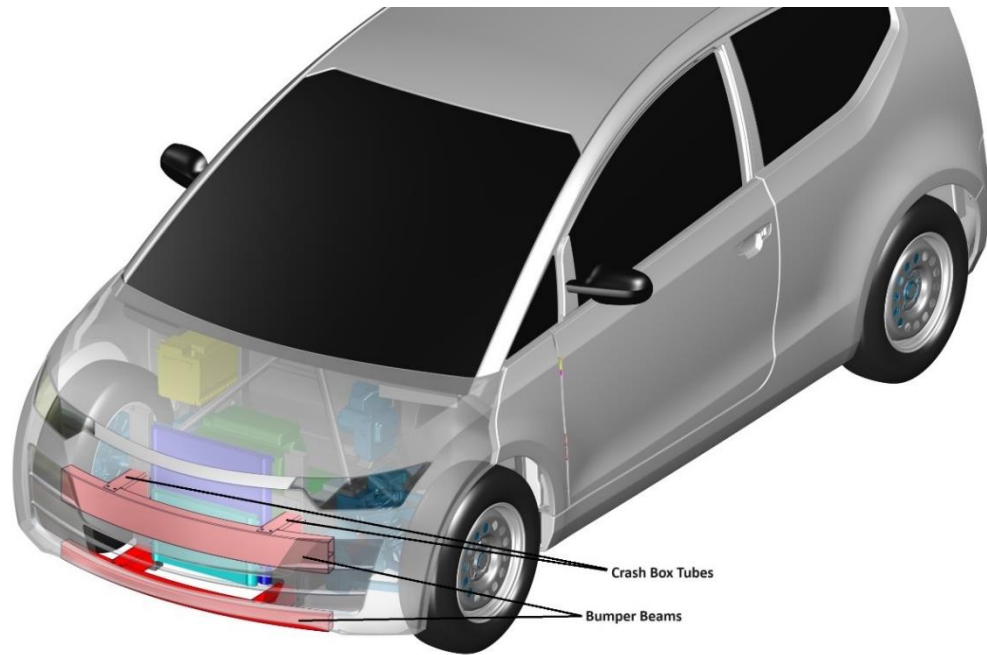


Figure 1.3. Crash boxes and front bumper beams are shown together on the car in red.

1.2. RESEARCH OBJECTIVES AND SIGNIFICANCE

In this master thesis, it is aimed to design the front crash system (FCS) in terms of crashworthiness, low cost and lightweight structure. Studies were carried out considering the objectives stated below.

- Lightweight Structure
- Design Parameters
- Improved Safety
- Reduced CO₂ Emissions

1.2.1. Lightweight Structure

From the engine block to the body in white (BIW) parts of the vehicle, from the chassis to the skeleton, steel is the most used metal in a vehicle. Features such as being easy to form, being relatively cheaper to produce than other metals, high strength, and being able to maintain its form for many years after shaping have made steel the most used main material in an automobile.

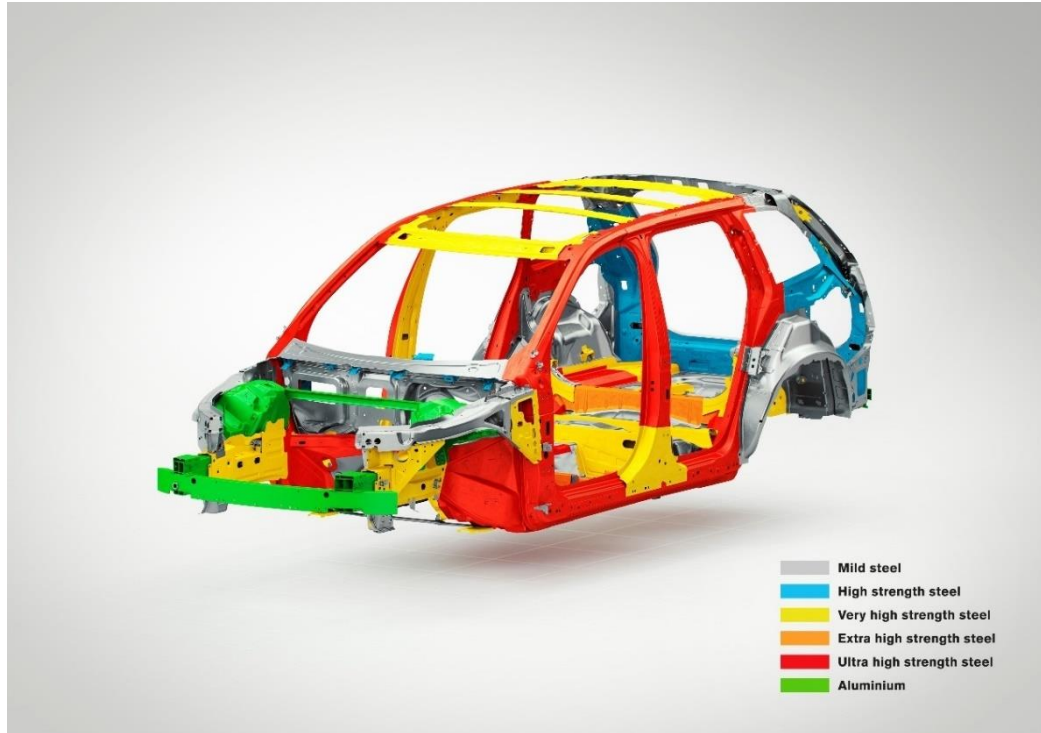
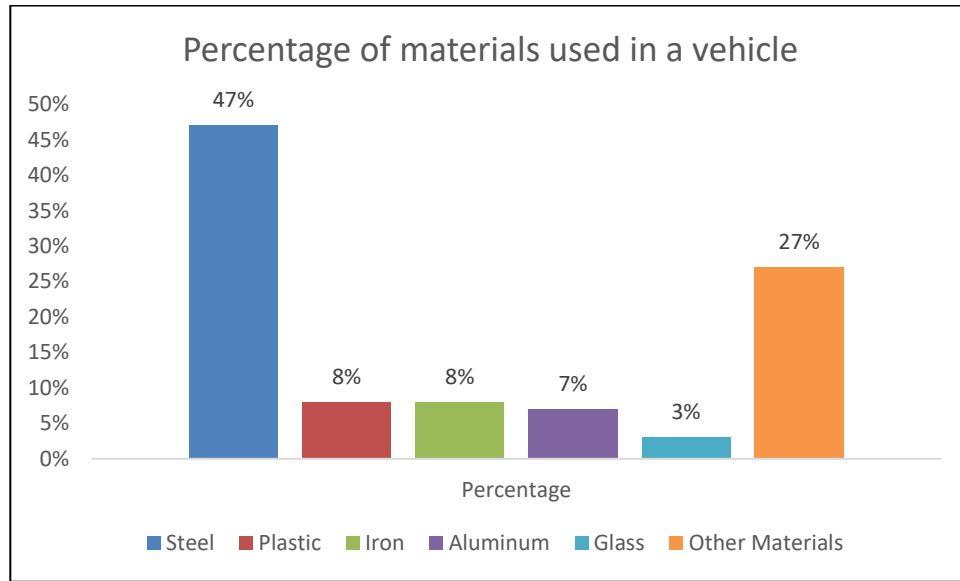


Figure 1.4. Steels used in the Volvo XC40 model [2].

The environmental damage caused by vehicles, especially global warming and carbon emissions, has begun to push manufacturers to conduct new research. To prevent environmental disaster, governments and the World Health Organization (WHO) have issued new regulations to reduce carbon emissions in vehicles. Many R&D studies, including weight reduction studies, have been initiated to reduce the CO₂ emissions released into the environment in vehicles. Weight reduction efforts in vehicles first started with topological optimization studies. With the R&D studies, parts with the same strength value but taking up less space in volume began to be preferred. With the development of modern manufacturing methods such as additive manufacturing after traditional manufacturing methods, topology optimization studies have accelerated and diversity has increased. In particular, the development of the aviation industry and the production of modernized fighter and passenger aircraft have become possible with the development of lighter and stronger materials than steel. Composite materials, magnesium and carbon reinforced aluminum alloys have gained an important place in the automotive, aviation and defense industries.

Tablo 1.2. Percentage of materials used in a car.



1.2.2. Design Parameters

The parameters that make up the design are the most important elements in order to reveal the right design. The design should be made after the most optimum design parameters are found. In general, if the design passes the testing stages after it is first made, it is produced and added to the assembly. Necessary R&D work is carried out on the produced part and weight reduction studies are carried out.

Topology optimization has a very important place in industries where low tolerance and high precision parts are produced, such as the aerospace, automotive and defense industries [3]. Using optimized parameters in the design phase eliminates problems that may occur after production and allows the part to be used without the need for redesign. The tolerance value in the aviation industry is 0.001, and the parts that require the most precision among all industries are produced in the aviation industry. Topology optimization studies have been used extensively by researchers in recent years and the number of studies is increasing. Munk et al. developed an optimization method to be used in the design of the hypersonic aircraft wing, thus ensuring that the aircraft wing was designed with the most accurate parameters during the design phase [4]. When Zhu compared the topology optimization study he carried out in the field of stretch forming die with traditional production methods, he observed that there was a

decrease in stress and displacement values [5]. Additive manufacturing method also offers innovative solutions in the production of automotive parts, and topological optimization studies are also carried out in this production method [6,7].

Crash box tubes and bumper beam designs also consist of various parameters. In this thesis, tests were carried out using finite element analysis (FEA) to find the correct design parameters while designing tubes and beams.

Parameters that make up the crash tube and bumper beam design;

- Cross section of the tubes
- Thickness



Figure 1.5. Circular cross-sectional crash tube with groove stamp.



Figure 1.6. Rectangular cross-sectional tapered crash tube with double groove stamp.

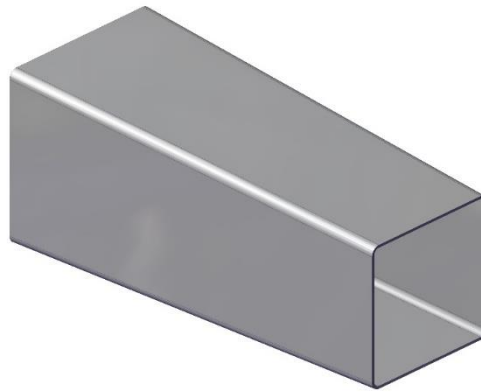


Figure 1.7. Rectangular cross-sectional tapered crash tube

The negative and positive effects of geometries such as grooves and cutouts on the energy absorption of the tubes will also be studied. The possible effects of such geometries on energy absorption have been concluded by studies conducted by researchers [8,9].

1.2.3. Improved Safety

The aim of the study is to provide a safer driving environment for the passengers in the vehicle. Since the kinetic energy occurring in high-speed accidents is very high, the crashworthiness of the tubes decrease considerably.

1.2.4. Reduced CO₂ Emissions

Although materials such as iron and steel are used as main materials, aluminum and its alloys, composite materials, carbon fiber materials, polymers, etc. As the use of lightweight materials increases, vehicle weight decreases. With the use of lighter but stronger materials than iron and steel, carbon emissions in vehicles have decreased. Thus, the use of zero emission vehicles (ZEV) has increased [10].

1.3. RESEARCH QUESTIONS

At the end of this thesis you will find the answers to the following questions.

- What is the best polygonal cross-section in terms of energy absorption?
- Energy absorption of multi-cell front bumper beams and crash tubes compared to traditional thin-walled single-cell structures.

1.4. LIMITATIONS

Since this project was done using numerical simulation, it is not known how it will behave in real conditions. Since this project was done using numerical simulation, it is not known how it will behave in real conditions. The project was created entirely through theoretical research and verification by computer aided engineering (CAE).

1.5. RESEARCH PURPOSE

The main purpose of this study is to make the optimum design of crash box tubes and front bumper beams in terms of strength/weight ratio. As a result of the analysis of the designs, the design will be completed by selecting the part with the best power/weight ratio.

1.6. TYPES OF CRASH TESTS

There are many crash test performed by Euro NCAP and the most famous ones are [11];

- Frontal Collision
 - Full width frontal collision (FWFC)
 - Offset frontal collision (OFC)
- Lateral Collision (LC)
- Roll Over Collision (ROC)

1.6.1. Frontal Collision

Frontal crashes have the highest fatality and injury rate among the other three types of crashes. FWC occurs when two vehicles coming from opposite directions collide head-on. The purposes of performing such tests are to predict the forces that may occur to the passengers in the event of a collision and to see whether the kinetic energy generated at the moment of collision is distributed correctly to other parts of the vehicle. FWC consists of two separate tests. Thanks to the sensors connected to vehicles and test vehicles, various data are obtained and shared with companies. According to the test results, companies can carry out development work.



Figure 1.8. Frontal collision test of Chevrolet Camaro.

1.6.1.1. Full Width Frontal Collision (FWFC)

The FWFC test occurs when a test vehicle traveling at 50 km/h collides head-on with a vehicle traveling at 50 km/h. Additionally, a vehicle traveling at 50 km/h is tested by hitting a deformable wall weighing 1400 kg. The forces that the dummies positioned in the front and rear seats of the vehicle are exposed to at the time of the collision, the bending positions of the mannequins, and how much the airbag and FCS absorb the kinetic energy generated at the time of the accident are displayed through sensors.

1.6.1.2. Offset Frontal Collision (OFC)

Collision conditions are generally the same as FWFC. The reason why it is called offset is that the vehicle exposed to impact is hit from half of its front width, not its entire front width. For this reason, it is called OFC.



Figure 1.9. Full width collision of a vehicle tested by Euro NCAP with a rigid wall.

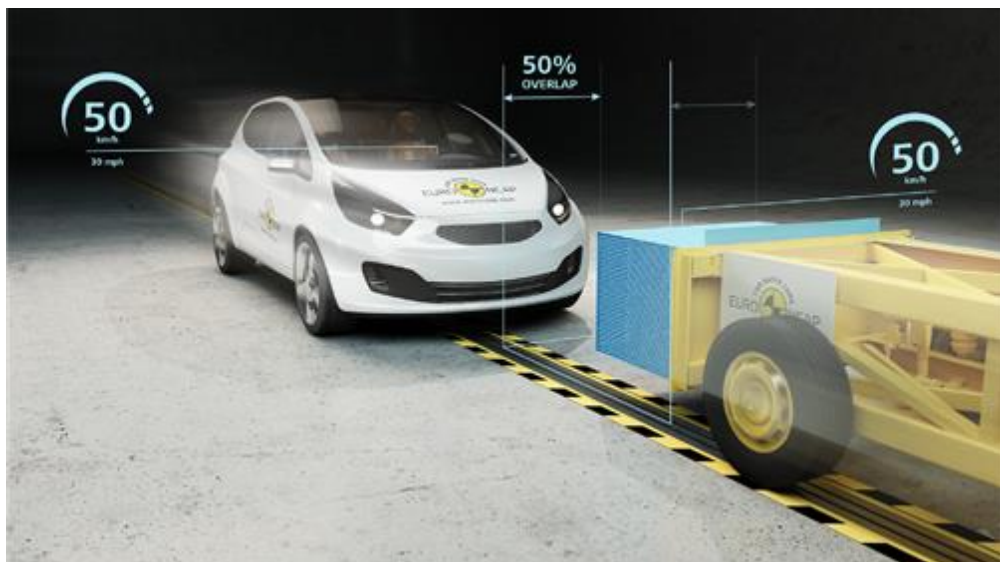


Figure 1.10. Offset frontal collision of a vehicle tested by Euro NCAP with a rigid wall.

1.6.2. Lateral Collision (LC)

Lateral collision is the second most common type of collision in which death and serious injuries occur. Compared to frontal collisions, there are fewer systems to absorb the energy, resulting in serious chest and head injuries to drivers. The tests are carried out by Euro NCAP. The static test vehicle is hit by a moving barrier at a speed of 60 km/h.

These lateral tests are extremely important because the sides of vehicles are the most vulnerable areas. Based on the results of these lateral tests, efforts are being made to further develop the B-Pillar areas, to design and position the airbags in a way that is more protective and increases energy absorption, to deploy the airbags at the right time, and to ensure that the driver and passengers in the vehicle escape as undamaged as possible.

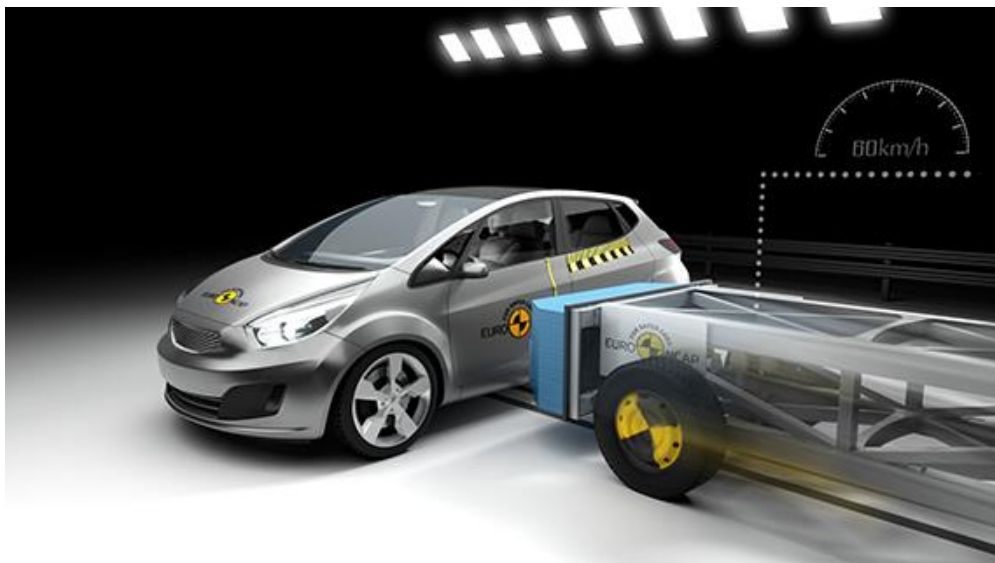


Figure 1.11. Lateral collision test between test car and deformable barrier.

In another test scenario, the moving test vehicle hits a stationary pole from the side and thus the effects of the collision on the vehicle are observed. The results are evaluated correctly, and the protective systems of the vehicle are strengthened with the necessary R&D studies.



Figure 1.12. Lateral collision test between test car and rigid pole.

1.6.3. Roll Over Collision

Negative situations and unprotected areas in vehicles that rolled over or were hit by the roof are tested.



Figure 1.13. Roll over collision of the test car.

PART 2

LITERATURE REVIEW

A crash box is one of the important parts of vehicle safety. The crash box is a mechanical part located between the vehicle body and the bumpers. It is designed to significantly reduce the energy transmitted to other mechanical parts of the vehicle by absorbing the energy released during impact [12]. Bumper beams are located in front of the car and rear as well, they are also one of the most significant components of a car that protect passengers and vehicles from severe injuries and collapse [13]. With the development of technology, there are also developments in the automobile industry and investments are increasing seriously. Thanks to investments and technology, serious studies are carried out in the field of vehicle safety.

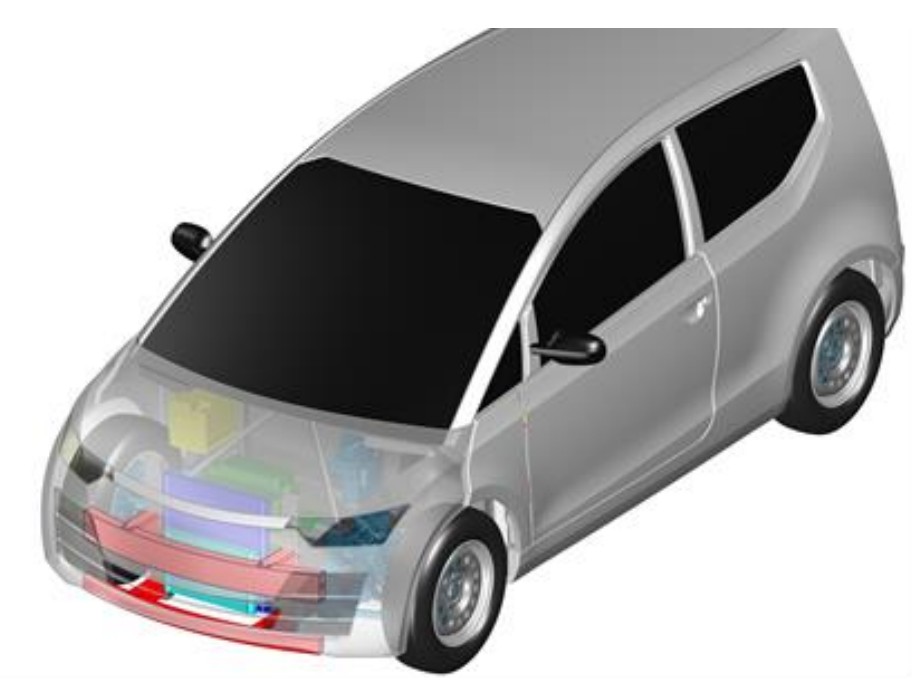


Figure 2.1. Crash box tubes and bumper beams shown in red.

Most of the theoretical and experimental optimization studies have been done in the structural geometry and design parameters field. Cross-section, wall thickness, angle,

and inducing grooves are some of the most optimized design parameters. Many studies have been carried out in this headlight until today and it continues to be done. Farkas et al. [14] studied optimizing the front bumper system with the fuzzy finite element method and improved the parameters & geometry.

Segade et al. [15] performed studies to design the most optimized crash boxes in respect of buckling shape modes. Their study investigated only squared cross-sectional tubes, and variables such as wall thickness and material stiffness were also compared to find their effect on crash boxes. To establish a connection between previous similar works they kept some values the same as the previous ones such as 15 km/h of velocity and 250 kg of weight which means the plate crashes with the crash boxes with 2.17 kJ of kinetic energy. The study observed that by reducing the wall thickness from 1.6 mm to 1.3 mm, the lower the wall thickness, the lower the folding resistance. They used four different materials to compare results such as Steel S355, Steel S255, Aluminium AA6060 T4, and Aluminium AA6060 T6. It was found in their study that the most convenient wall thickness values are 1.4 mm, 1.6 mm, 2.00 mm, and 2.6 mm respectively. Finally, it was obvious that Aluminium AA6060 T6 absorbed more energy than steel with 8991 KJ/kg. Eyvazian et al. [16] examined the crashworthiness of aluminum alloy corrugated metal-composite tubes with 1.5mm of thickness and 70mm height under quasi-static axial conditions. Filament composite covering is used for the metal-composite process.



Figure 2.2. Specimens used in the tests [16].

S: Simple tube (left)

SWCD: Corrugated tube (middle)

CWCD: Composite covered corrugated tube (right)

Corrugated tubes showed plastic deformation under loading. It was found that adding composite to the corrugated metal increased the energy absorption by 53%.

Tablo 2.1. Experimental results of tests [16].

	S	SWCD	CWCD
Mean load (N)	2.08E+04	1.22E+04	3.45E+04
Absorbed Energy (J)	1.04E+03	6.10E+02	1.73E+03
Specific Absorbed Energy (J/g)	1.35E+01	7.92E+00	1.21E+01

Wang et al. [17] created a novel negative Poisson's ratio (NPR) beam and an NPR absorber to explore the structure's crashworthiness behavior. NPR structure includes many hexagonal cellular structures inside of it. Becoming wider when pulled and becoming thinner when compressed makes NPR structures special and unusual [18]. High energy absorption, lightweight, and resistance against impact are some of its other important features. They changed the rigid bumper beam (Fig.15) with an NPR bumper beam.

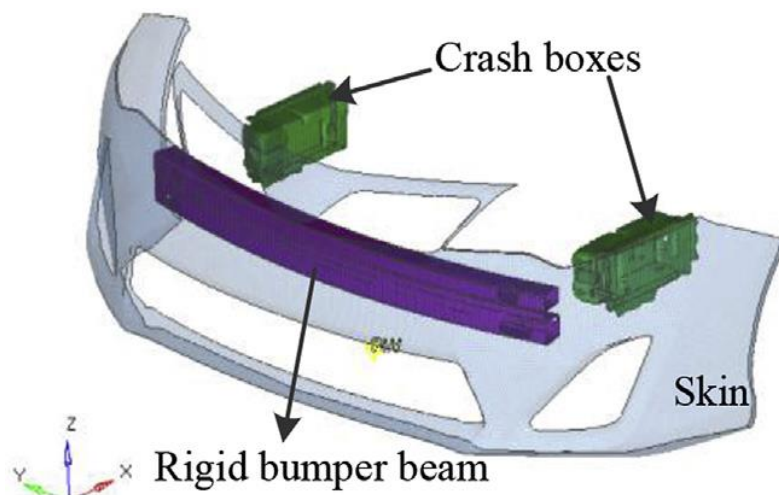


Figure 2.3. The traditional front bumper system of a car [17].

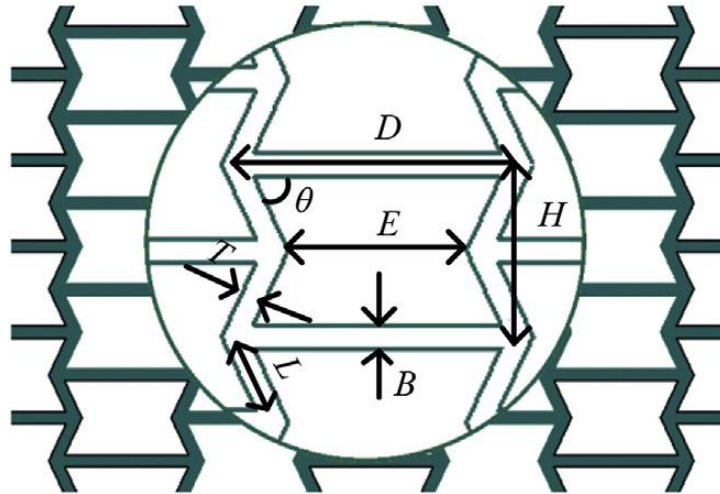


Figure 2.4. Hexagonal cells and parameters of NPR structure [17].

They optimized their NPR BUMPER structure with an electronic-search algorithm (ESA) and a non-dominated sorting genetic algorithm (NSGA-II). (Fig.19)

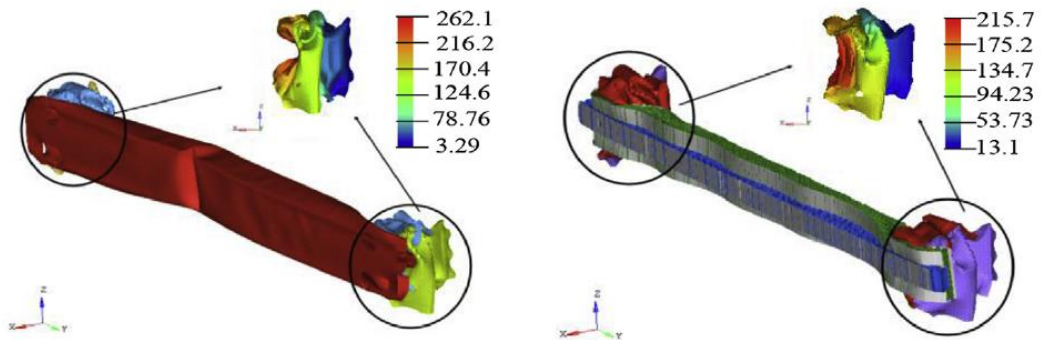


Figure 2.5. The initial rigid bumper beam (left) and the NPR bumper beam are revealed. (right) [17].

It was found that the ESA algorithm method gives better results than the NSGA-II optimization method. With the ESA algorithm, the mass of the bumper system is reduced by 0.12 kg. The impact force of the rigid wall is reduced by 10.3 kN with the ESA as well [17].

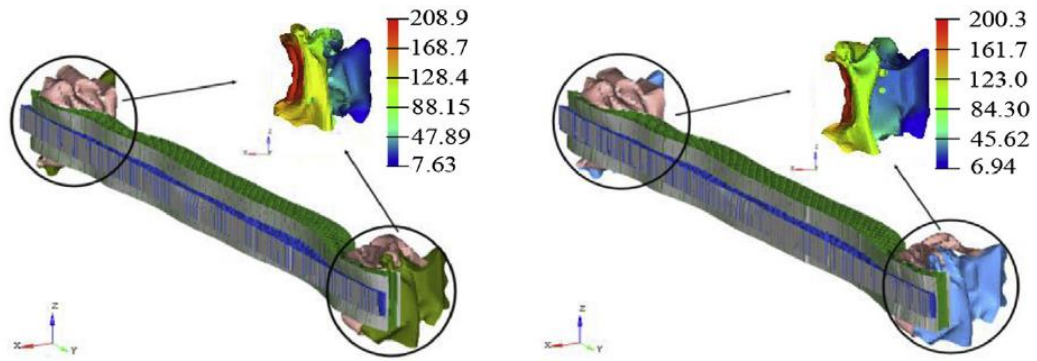


Figure 2.6. Deformation of NSGA-II optimized bumper (left) and ESA optimized bumper beam. (right) [17].

Yang et al. [19] analyzed thin-walled squared cross-sectional tubes in terms of crashworthiness under oblique impact loading. They studied to optimize the parameters such as geometry, impact angle, and material to reach the desired final structure. Aluminum alloy AA6063 T6 was used for the thin-walled tubes and the foam was also made of aluminum as well. The lower cross-section width, wall thickness, material yield strength, and foam material density reduce the peak crushing force (PCF) for both empty and foam-filled tubes. Zahran et al. [20] made a novel tailor-made crashworthiness optimization study by combining multiple techniques into a single study. They analyzed squared cross-sectional tubes under axial and quasi-static impact loading.

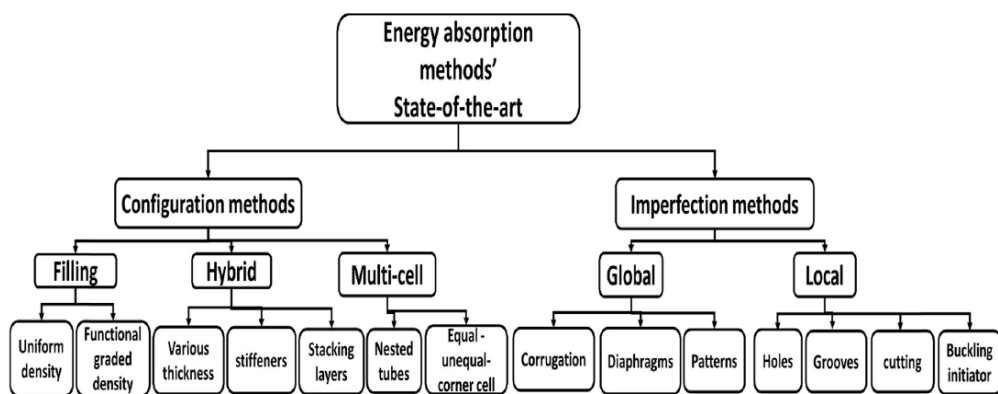


Figure 2.7. Energy absorption methods [20].

Their novel tube is named tailored multi-stage square tubes (MSSQ). Aluminum alloy AA6061-O was used for all the specimens. Conventional square (CSQ) tube,

conventional tri-tubular tube (CTSQ), and MSSQ compared each other in terms of crashworthiness. (Fig. 14) It was found that MSSQ absorbs more energy than CSQ and CTSQ by 56.3% and 28.7% respectively. It also increases the crushing efficiency by 36.6% and 22.1% compared to CSQ and CTSQ respectively [20].

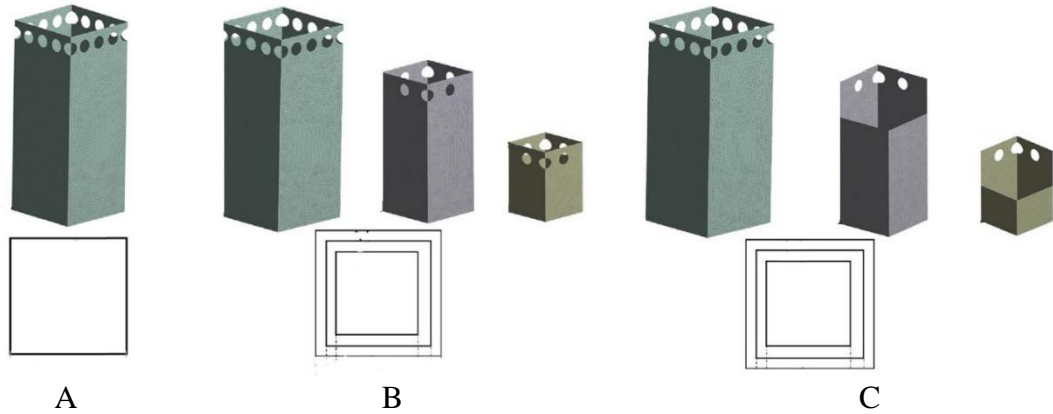


Figure 2.8. MSSQ (A), CSQ (B) and CSTQ (C) structures [20].

Liu et al. [21] studied the effect of the position ratio of the foam on the energy absorption under the axial impact loading of cylindrical tubes filled with foam material. All tubes were made of aluminum alloy AA6061T4. Single-cell and double-cell tube structures filled with negative (NPR) and positive Poisson's ratio (PPR) were analyzed to observe their crashworthiness. A new structure, the sandwich double tube filled with mixed Poisson's ratio (MPR), was created by combining NPR and PPR. Results show that the sandwich double tube filled with MPR foam possesses better specific energy absorption (SEA) compared to PPR and NPR structures.

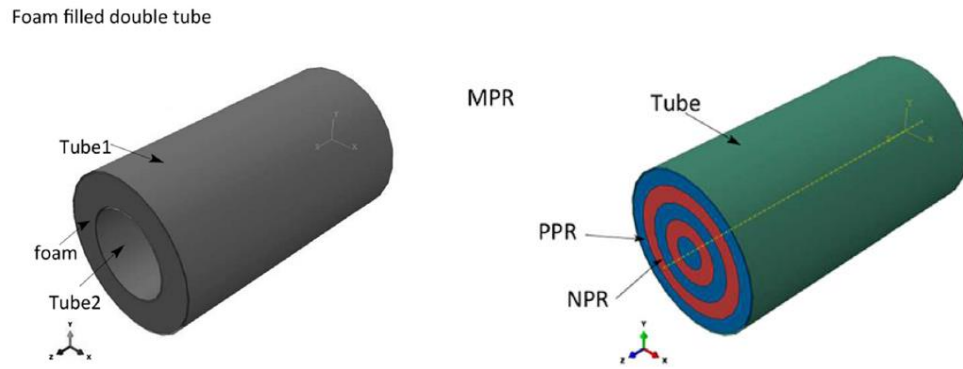


Figure 2.9. Representation of the MPR structure (left) and foam-filled double tube (right) [21].

Altin et al. [22] studied to optimize the crashworthiness of foam-filled multi-tubular thin-walled circular tubes under quasi-static impact loading. In their study, both axial and lateral foam filling was applied to the structures and compared to each other.

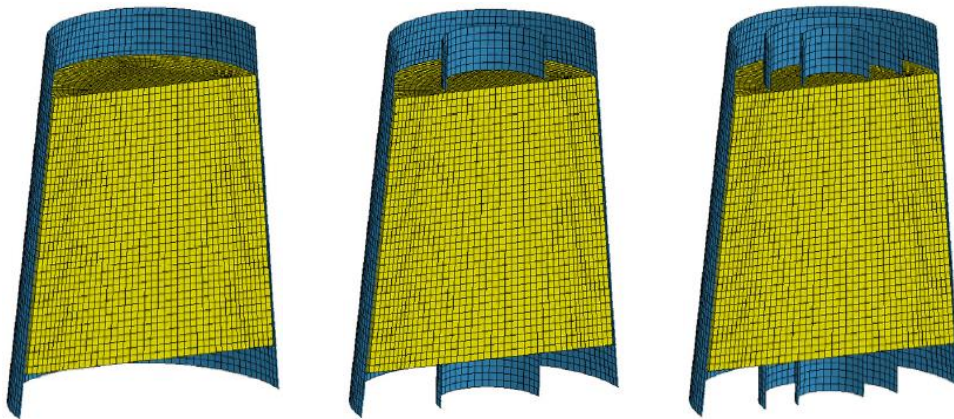


Figure 2.10. Mono-tubular (left), bi-tubular (middle), and tri-tubular axial foam-filled circular tubes with different foam heights [22].

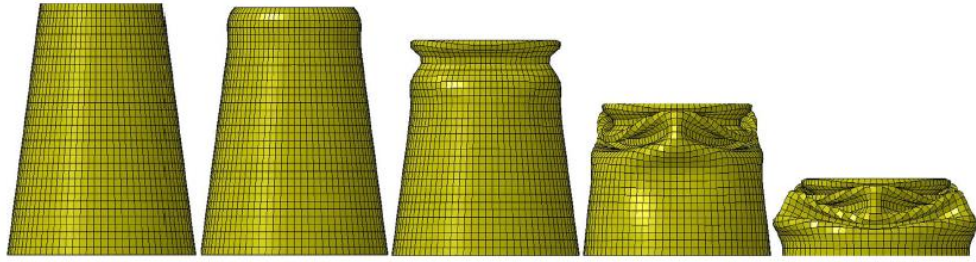






Figure 2.11. Deformation of lateral foam-filling circular tubes [22].

Wall thickness, draft angle, density, diameter, and height of the foam were their parameters to be optimized. Response surface-based topology optimization was performed for crash force efficiency (CFE) and specific energy absorption (SEA). In conclusion, it was found that the maximum SEA with lateral foam-filled tubes was 6% bigger than the axial one. For the lateral foam-filling tube, the optimum variables are 0.820 g/cm³ of the density of the foam for CFE and 0.628 g/cm³ for the SEA, 40.7 mm of tube diameter, 7.5° draft angle, and 1.7 mm wall thickness. For the axial foam-filling tube, the optimum variables are 0.820 g/cm³ of the density of the foam for CFE and 0.628 g/cm³ for the SEA, 75.5 mm of foam height, 7.5° draft angle, and 1.7 mm wall thickness [22]. Wang et al. [23] studied the crashworthiness of Koch structures with single-wall and double-wall. All specimens were made of aluminum alloy 6061-O. Koch fractal (KF), circular Koch fractal (C-KF), and hybrid Koch fractal (H-KF) structures were grouped in 1st order, 2nd order, and 3rd order and then analyzed.

Tablo 2.2. Representation of Koch structure curves with orders [23].

Fractals	Order n	Edge length L_n	Edge number Q_n	Perimeter length S_n
	0	L_0	1	L_0
	1	$1/3L_0$	4	$4/3L_0$
	2	$(1/3)^2L_0$	4^2	$(4/3)^2L_0$
	3	$(1/3)^3L_0$	4^3	$(4/3)^3L_0$

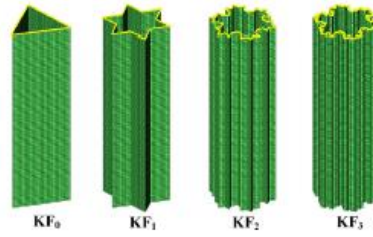


Figure 2.12. Koch fractal (KF)(green) structures illustration [23].

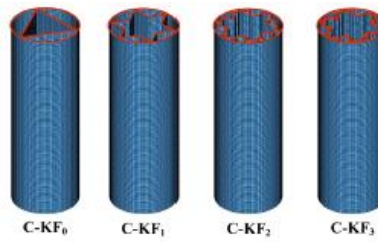


Figure 2.13. Circular Koch fractal (C-KF) (blue) structures illustration [23].

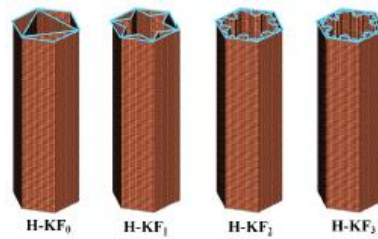


Figure 2.14. Hybrid Koch fractal (H-KF) (brown) structures illustration [23].

Results show that the 2nd order Koch fractal structure increases the energy absorption of the tube. The 2nd order structure's crashworthiness is better than the ones that have the same mass multi-cell thin-walled structures. 2nd order H-KF structure with .4 mm of wall thickness absorbed 39.12 KJ/kg energy and was chosen as the most optimal structure [23].

LI, Zhixiang, et al. [24] worked on the crash analysis of multi-cell square corrugated tubes made of aluminum alloy AA6061O. Their study came up with a new type of crash tube called “multi-cell circumferentially corrugated square tubes” (CCSTs). It can be seen in figure 28 that their specimens consist of multi-corrugated geometries and multi-cells.



Figure 2.15. Specimens used by LI, Zhixiang [24].

According to the results of their studies, as the number of cells increases, the mean crushing force (MCF) increases as well. It was also found that tubes with multi-cell had better performance than traditional ones in terms of specific energy absorption (SEA), crushing force efficiency (CFE), and MCF.

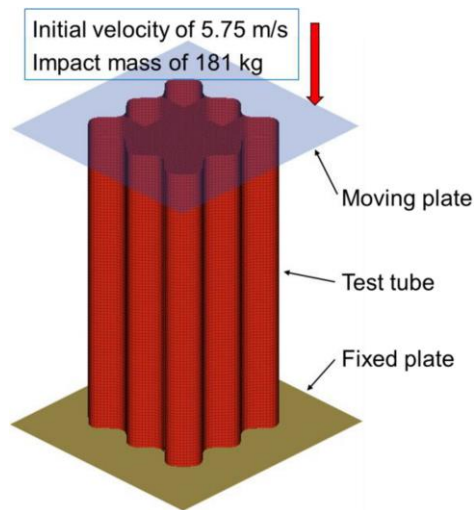


Figure 2.16. FEA model of CCST [24].

With advances in materials science, components used in the automotive industry can be produced with greater strength and be lightweight. Composite materials and metal alloys such as aluminum alloy are mostly used for crash box production [8].

Kurtulus et al. [25] studied how to convert an aluminum crash box front bumper system that is produced in a mass production system into a magnesium alloy front crash bumper system via the design experience method. In addition to being the lightest metal known, they preferred magnesium of its easy machinability, better surface finish than other metals, low cutting forces, and easy chip flow. Since the studies using magnesium alloy in this field are very limited, the study is very important. 4 design parameters were so important for their studies to optimize and reach the desired data bumper beam ribs, the wall thickness of the bumper beam, bumper beam middle width, and wall thickness of the crash box. At the end of their study, they managed to improve the crash box performance by about 20% in terms of energy absorption and managed to reduce the weight of the design by about 15% by using magnesium alloy compared to aluminum alloy. This study observed that crash boxes produced with magnesium with a circular cross-section, a material lighter than aluminum, absorb more energy when the right parameters are used. The weight of the system produced using magnesium alloy was 3218 grams and absorbed 10.34 kJ of energy, while the weight of the system produced with aluminum alloy was 3741 grams and absorbed 9.97 kJ of energy. Li et al. [26] studied lightweight crashworthiness optimization on the crash box, front rail, and bumper. Firstly, they replaced the materials used in the crash box, front rail, and bumper with materials TRIP800, DP800, and aluminum alloy 6060 respectively. They filled the crash box and bumper with aluminum foam to increase crashworthiness and energy absorption. According to the test results, they compared the results of the assembly consisting of a crash box, front rail, and bumper, using a single material, and using the above-mentioned materials. The crash test was carried out with a 20 km/h impact velocity. They succeeded in reducing the total mass by 11.1% and increasing the energy absorption by 10.1%. They also achieved that the folding distance and peak crash force decreased by 12.6% and 11.1% respectively. The load applied to the bumper during a crash causes the bumper to bend in the middle and creates a great disadvantage. In the multiple materials optimization stage, it was found that the bumper filled with aluminum foam prevents the bumper from bending in the middle and the system absorbs more energy. Composite materials are also used in this field and various studies have been carried out. Fuchs et al. studied composite materials to reveal composite's economic advantages over other metals used in the automotive industry. These materials are

easily producible, resistant to corrosion, and lightweight materials [27]. Boria [28] studied the design of carbon fiber-reinforced plastic (CFRP) structures for crashworthiness applications. The material he used for his project is prepreg which is acquired from high-strength carbon fibers. He investigated truncated conical geometry and Formula SAE front attenuator geometry's crashworthiness behavior under crash conditions by applying quasi-static and dynamic tests. As a result, he found that both crash boxes exposed axial load under quasi-static and dynamic tests showed no difference in terms of displacement. Energy absorption of conical structure reduced notably at the quasi-static test in comparison with the dynamic test.

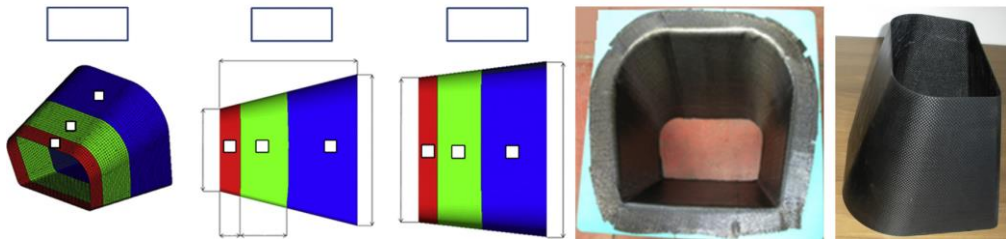


Figure 2.17. Front attenuator model of Formula SAE car [9].

Rao et al. [29] analyzed the crashworthiness of bumper systems with different materials. Aluminum alloys such as AA7003-T79, AA7003-T1, and AA6060-T1 were used in the tests. It was found that all structures absorbed the energy transmitted to the bumper, with alloy AA7003-T79 deformed the least. This alloy structure also showed high stiffness compared to other alloys. Thus, they concluded that the most suitable material is the AA7003-T79 alloy between three alloys. Reyes et al. [30] used various polymer foam materials with different densities as core material and steel as covering material to investigate the sandwich structure's behavior in terms of crashworthiness under quasi-static tests. The MCR consists of 8mm thickness of DOCOL 600DL steel as covering material and 50mm thickness of different polymer foam materials with various densities as core material such as extruded polystyrene (XPS) and expanded polypropylene (EPP) with densities between 28-45 kg/m³ and 20-200 kg/m³ respectively.

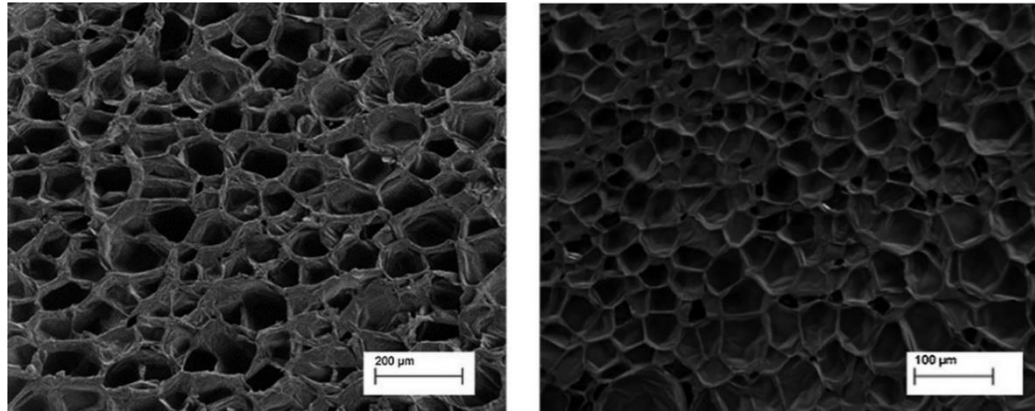


Figure 2.18. Microstructure images of XPS-400 left and EPP-5130 right [30].

They found that both foam materials showed viscoelasticity behavior and recovered themselves when the load was removed. Among the XPS and EPP foam materials with the same density, XPP absorbs more energy than EPP foam. Both foam materials were considered isotropic after quasi-static tests' results. XPS is preferable as a core material in terms of minimum weight and energy absorption whereas EPP is preferable if displacement and less amount of force transmitted to the bumper system are important. Gronostajski et al. [31] compared thin-walled structures made of AZ31 magnesium alloy with the DC04 and HC380LA steel thin-walled structures. In addition, they filled the structures with aluminum foam to increase energy absorption. It was found that HC380 steel can be used in structures produced for energy absorption whereas DC04 steel is not suitable for such structures. It was also observed that structures made of HC380 steel fold more regularly than structures produced with DC040 during impact. The aluminum foam-filled structure absorbed more energy than others as expected.

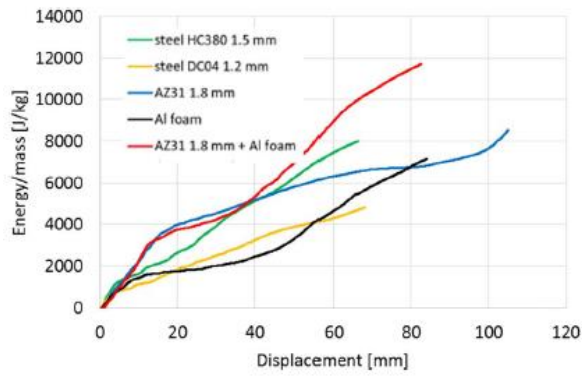


Figure 2.19. Energy/mass and displacement table of materials used in the tests [31].

Tablo 2.3. Mass comparison of the structures [31].

Material	Mass (g)
Steel HC380 1.5 mm	452
Steel DC04 1.2 mm	366
AZ31 1.8 mm	125
Al. foam	102
AZ31 1.8 mm + Al. foam	227

Dirgantera et al. [32] examined square cross-sectional aluminum foam-filled tubes in terms of crashworthiness with the strain rate of the foam. Single-walled and double-walled square cross-sectional tubes filled with aluminum foam and effects were observed.

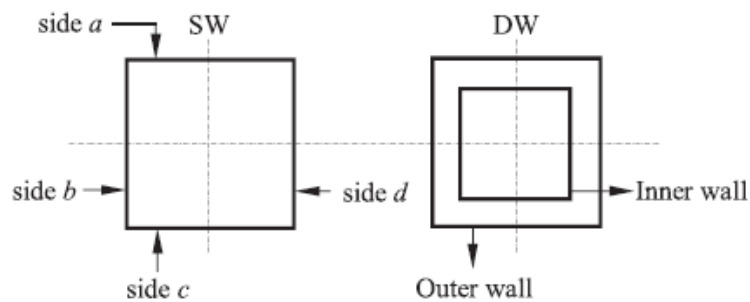


Figure 2.20. Cross-sections of single/double-walled (SW/DW) tubes [32].

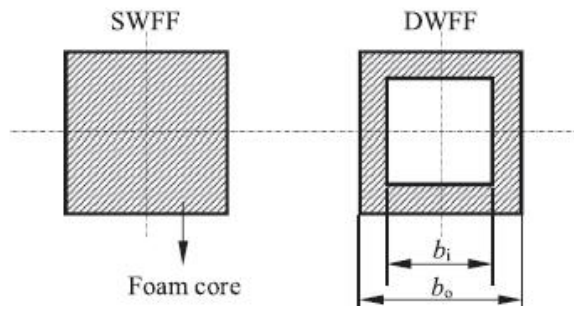


Figure 2.21. Single/double-walled (SWFF/DWFF) foam-filled tubes [32].

Tube walls were produced with Aluminum alloy AA6063 T1. Aluminum foam ALPORAS was used to fill the tubes. ALPORAS is an ultra-light aluminum foam and can absorb sound as well as energy [33].

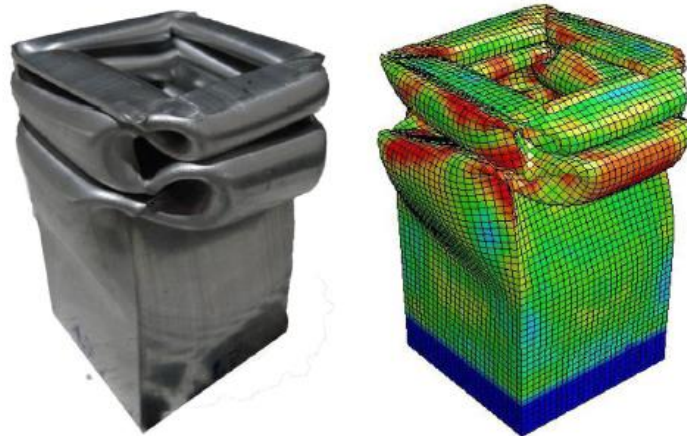


Figure 2.22. Deformation shapes of SW [32].

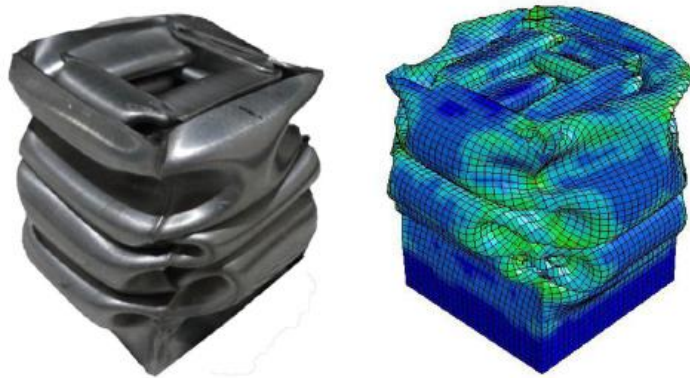


Figure 2.23. Deformation shapes of DW [32].

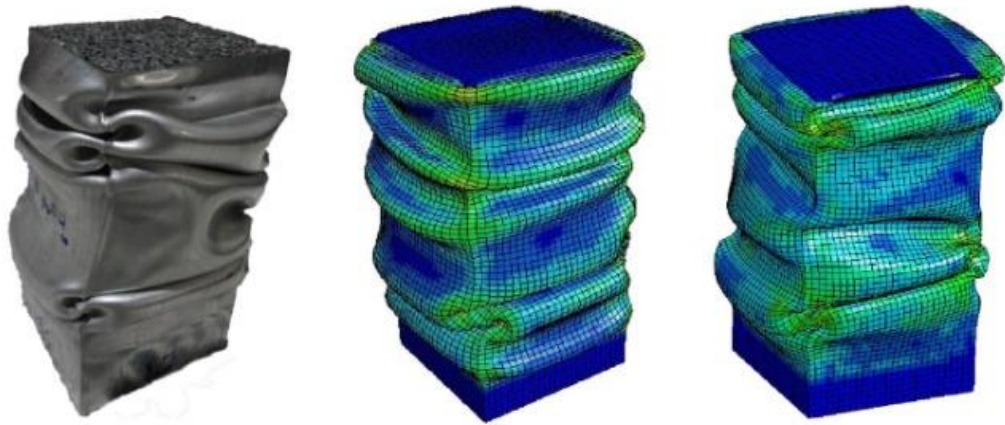


Figure 2.24. Deformation shapes of SWFF [32].

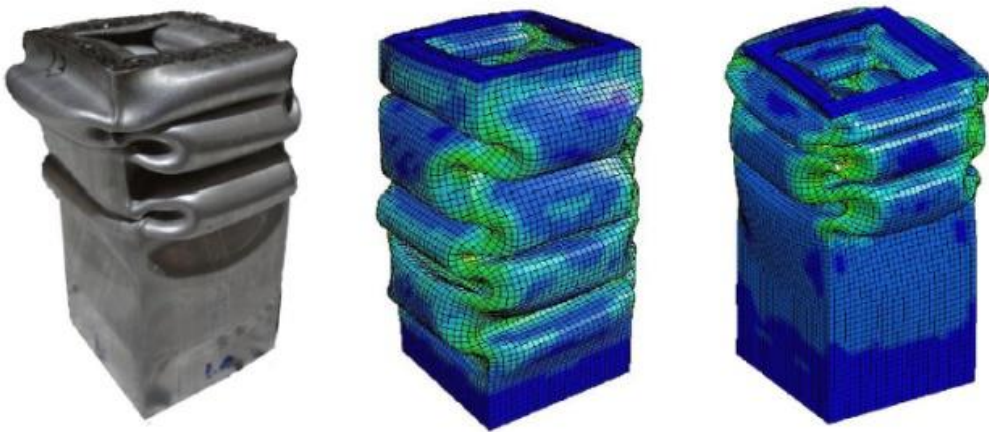


Figure 2.25. Deformation shapes of DWFF tubes [32].

Experimental and numerical tests found that inserting aluminum foam into tubes increases energy absorption. It was also recommended that considering of strain rate of foams will predict the tubes' crashworthiness behavior better in numerical methods. Mean crashing force with SWFF was improved compared to SW and same manner with the double-walled ones [32].

Tanlak et al. [34] studied to optimize the crashworthiness of bumper beam structure. In their study, the impact velocity is 64km/h and 40% offset impact conditions. They reached the desired optimized beam structure with a hybrid model by combining Nelder&Mead and Genetic algorithm methods. This study can be categorized under loading conditions.

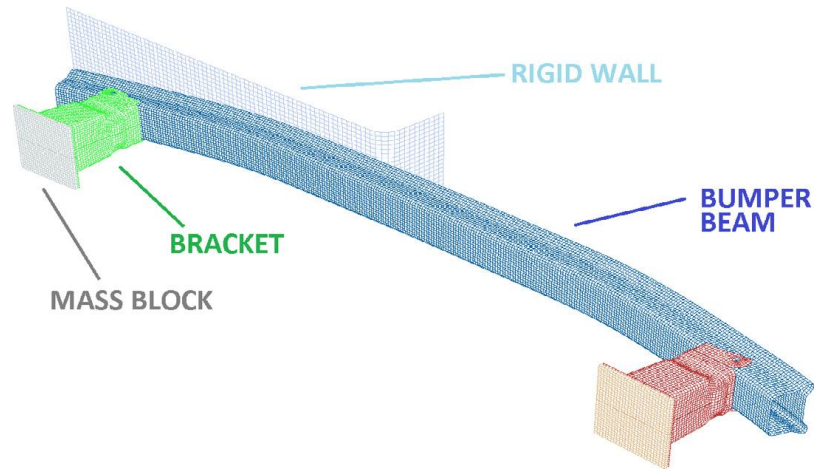


Figure 2.26. Assembly of the front crash system with mass blocks [34].

The variables to be optimized were the variables that create the beam's cross-section. In conclusion, their optimized bumper beam showed great performance in comparison with the original bumper beam cross-section in terms of energy absorption.

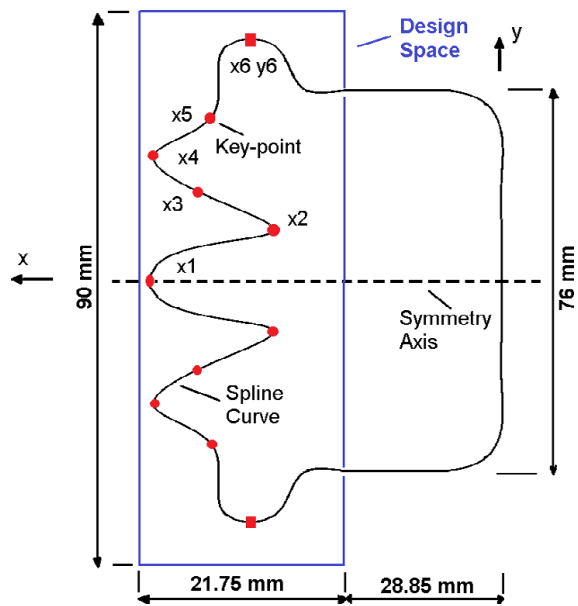


Figure 2.27. The variables to be optimized [34].

OPTIMAL SHAPES			BENCHMARKS		
w1=1, w2=0	w1=0, w2=1	w1=0.8, w2=0.2	Currently in use	Rectangle	Dome

Figure 2.28. Optimal bumper beam cross-sections (left) and the original ones. (right) [34].

Tran et al. [35] studied the multi-cell crash box geometries made by aluminum alloy under dynamic oblique impact.

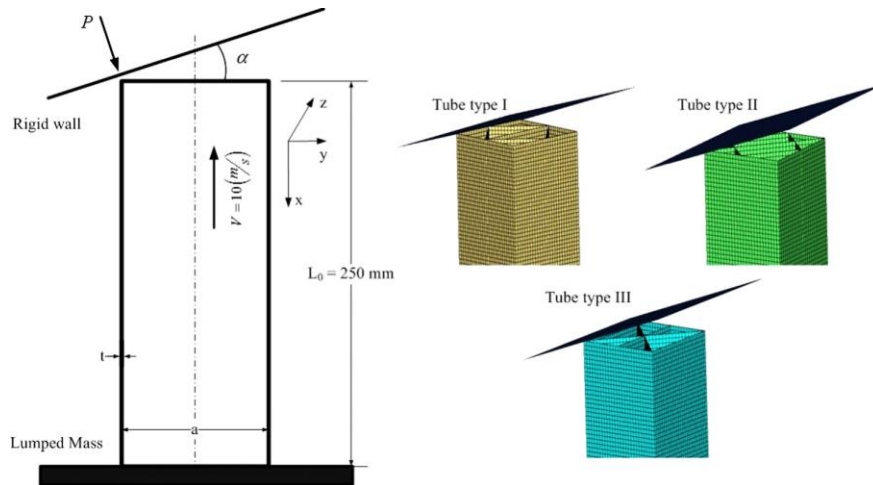


Figure 2.29. FEA model representation and multi-cell geometries' cross-sections used by Tran [35].

Table 6 shows the optimal results for the wall thickness, angle, SEA, and PCF for Aluminum Alloy AA6060 T4 material tubes.

Tablo 2.4. Optimal values for three types of crash tubes in terms of Specific Energy Absorption (SEA) and Peak Crashing force (PCF).

Type of cross section	Terms	Optional design variables (mm)	SEA (kJ/kN)	PCF (kN)
Type I	Approximate value FE	t=1.4, a=80	14.378	98.253
	analysis value		14.279	98.779
	RE		0.693	-0.259
Type II	Approximate value FE	t=1.43, a=80	16.746	107.631
	analysis value		16.607	107.093
	RE		0.837	0.502
Type III	Approximate value FE	t=1.48, a=80	14.095	106.681
	analysis value		14.151	106.532
	RE		-0.396	0.140

There are many studies on this subject and table 2.5. shows some of the studies in summary form. Below studies in the list are classified into four categories: cross-sections of the tube, material used at the specimen, topic, and conclusion. While selecting the works in this list, attention was paid to ensure that they were different from each other and the above-mentioned studies.

Tablo 2.5. Other studies related to this thesis subject.

Cross-Section	Material	Topic	Conclusion	Reference
Hexagonal/multi-cell	Aluminum alloy AA6061	Thin-walled hexagonal tubes under dynamic crash loading are compared to each other. Connect to connect (C2C) and web to web (W2W) cross-sections are compared.	W2W has the best performance in terms of energy absorption. C2C had the worst among all specimens.	[36]
Circular/square	Aluminum alloy AA2024-T3	Calculation of the effect of uncertainties during progressive collapsing of circular and square tubes under axial loading.	The circular tubes have better performance than square ones in terms of crashworthiness. Elastic modulus is a very important quantity.	[37]
Circular/square/ellipse multi-cell	Aluminum alloy 6063-T5	Multi-cell tubes were evaluated in terms of crash force efficiency (CFE) and specific energy	Larger diameter and smaller wall thickness values are more important for CFE.	[38]

		absorption (SEA).		
Circular	Aluminum alloy 6061-T4/T6	Dynamic and quasi-static analysis of circular tubes made of AA6061-T4/T6 under axial loading.	AA6061-T6 and AA6061-T4 absorbed 5.96 kJ and 4.39 kJ energy respectively at quasi-static analysis.	[39]
Anti-tetrachiral, Hexachiral, hierarchical chiral	Aluminum alloy 5A06	Crashworthiness of chiral structures under different crashing scenarios.	As the impact speed increases the number of folds increases at chiral structures. Structures with square corners absorb the most energy and showed the best performance in terms of energy absorption.	[40]
Circular/square hybrid multi-cell	Aluminum alloy AA6061-O	Deformations and crashing behavior of hybrid structures.	Hybrid multi-cell structures with external circle shapes showed better performance than the external square-shaped ones in terms of deformation.	[41]
Square and octagonal	Aluminum alloy	The effects of lateral holes and their dimensions	Tubes with hexagonal lateral holes absorbed the	[42]

	AA6061-T4	on crashworthiness.	most energy and had the best crash results.	
Square/boundary controlled by cosine profile	Aluminum alloy AA6061-O	Crashworthiness of square corrugated tubes that its contour controlled by cosine profile.	Compared to traditional square tubes, corrugated tubes absorbed more energy with the same mass by 51.62%.	[43]
Rectangular open U tube spot-welded with plate	DP590 DP780	Tailor-welded blanks structures' optimization under dynamic load conditions.	As a result of their optimization studies, they succeeded in increasing the energy absorption ability of TBW structures by 3.5%.	[44]
The star-shaped structure between circular tubes named CSC-tubes	Aluminum alloy AA6061-T4	Crashworthiness of sandwich structures consists of star-shaped tubes between two circular tubes under axial impact loading.	According to the results, as the number of corners in star geometries increases, the amount of absorbed energy also increases. CSC-tube showed better	[45]

			crashworthiness results than individual structures such as two circular tubes and star-shaped tubes.	
Circular, rectangular, square, ellipse, hexagonal, octagonal	A36 Steel	Dynamic compression tests were applied to thin-walled structures with several cross-sections under axial and oblique impact loading conditions.	Among all specimens, the hexagonal cross-sectional tube performed the best performance in terms of energy absorption. Hexagonal cross-sectional tube with 2mm of thickness absorbed 26kj energy under 15m/s impact velocity. The same tube with foam-filled absorbed 30kj energy under the same impact loading.	[46]
Hexagonal	Aluminum alloy	Investigation of hexagonal	It was found that second-	[47]

	AA6061-O	structures containing inside hexagonal structures in terms of energy absorption.	order hexagonal structures improved the energy absorption ability of the structure by 289%.	
Circular, square, hexagonal	Aluminum alloy AA6060-T4	Crashworthiness performance of thin-walled tubes with circular, square, and hexagonal lateral cuts under dynamic axial loading.	Results show that windowed tubes present less peak crush force than traditional empty tubes. This result is an advantage for windowed tubes. However, windowed tubes are not preferable in terms of energy absorption and deformation because they absorbed less energy and had less deformation mode than simple tubes.	[48]
Circular/hybrid	Aluminum alloy	Investigation of a thin-walled	It was found that HCT	[49]

	AA6061-O	circular corrugated tube with decreasing number of grooves in terms of energy absorption. This type of tube was named hybrid corrugated tube (HCT) and compared the result with the ordinary corrugated one (OCT).	showed better results than OCT in terms of energy absorption.	
--	----------	--	---	--

PART 3

THEORETICAL BACKGROUND

3.1. FINITE ELEMENT METHOD

3.1.1. What is finite element method?

Finite element method (FEM) is a numerical technique in which a structure subjected to static, dynamic, thermal etc. loads is divided into small parts and each part is subjected to numerical calculations [50–52]. The finite element method works by dividing an object into a certain number of objects and each of these objects is called a mesh. Each of these meshes are combined and represents the part.

With the development of computer aided design (CAD), simulations made with the hand calculations were moved to the virtual environment and began to be used by engineers through computers and called computer aided engineering (CAE). Thus, stress distribution, deformation and displacement of solid mechanics under loads can be calculated [53].

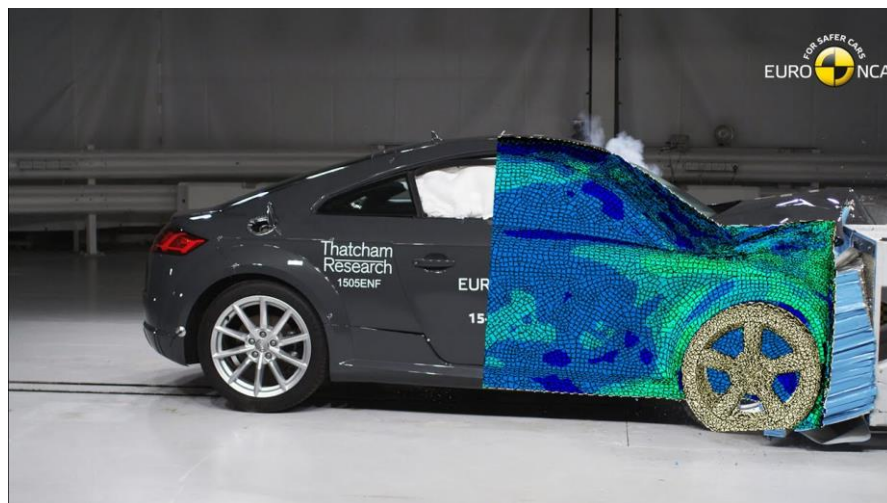


Figure 3.1. FEM representation of a car tested by Euro NCAP.

3.2.2. Governing equations of FEM's

$$[K]\{u\} = \{F\} \quad (3.1)$$

K= Global stiffness matrix

u= Nodal displacements

F= Nodal forces

Table 3.1. Governing equations of physical simulations [54].

	Property [K]	Behaviour {u}	Action {F}
Elastic	Stiffness	Displacement	Force
Thermal	Conductivity	Temperature	Heat source
Fluid	Viscosity	Velocity	Body force
Electrostatic	Dialectri permittivity	Electric potential	charge

3.2 SIMULIA ABAQUS/CAE

Abaqus (CAE) is Dassault Systemes' (DS) software that simulates physical mechanical systems under certain boundary conditions and loads using the finite element method. Abaqus provides high-precision simulation results for linear and nonlinear boundary conditions [55].

3.2.1. Simulation Steps

There are three steps in a physical simulation in every simulation softwares.

- Pre-Processing
- Solver
- Post-Processing

3.2.1.1. Pre-Processing

Pre-processing is the stage of making a mechanical part ready for simulation. After the pre-processing phase is completed, the part moves to the simulation phase and its behavior is monitored by exposing it to certain boundary conditions and loads using the finite element method [56–58]. At this stage, first the areas on the part that are difficult to mesh are made smoother and the sharp edges are rounded with as much radius as possible. Pre-processing consists of five stages.

1. Geometry preparation
2. Mesh
3. Boundary condition (BC)
4. Load
5. Constraint (if the design is an assembly)

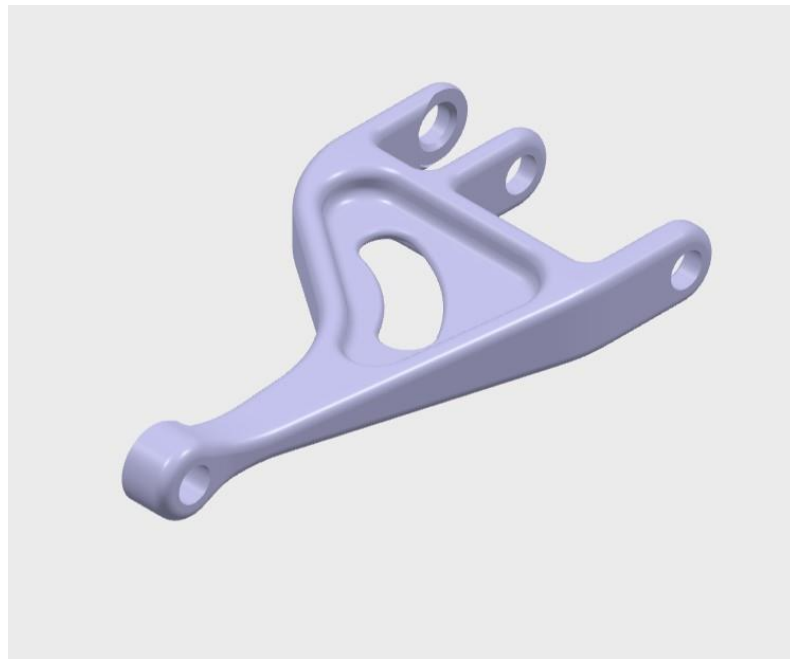


Figure 3.2. Physical appearance of the mechanical part to be simulated in the pre-processing stage.



Figure 3.3. FEM appearance of the mechanical part to be simulated in the pre-processing stage.

3.2.1.2. Solver

FEM simulation of the prepared mechanical part is done at this stage.

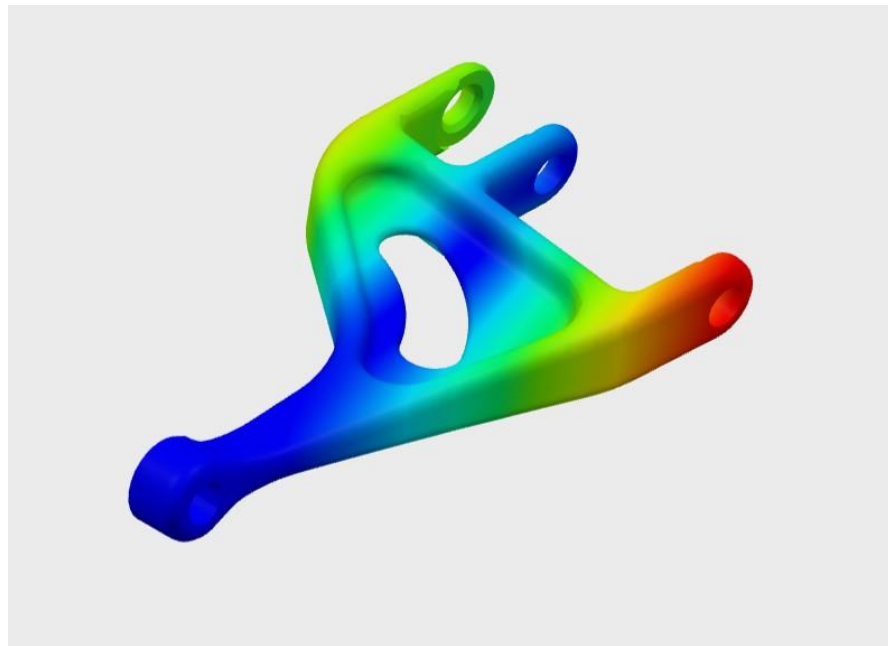


Figure 3.4. Stress distribution of the simulated part under loading.

3.2.1.3 Post-processing

This is the stage where the results such as stress distribution, displacement, deformation etc. of the simulated part are evaluated.

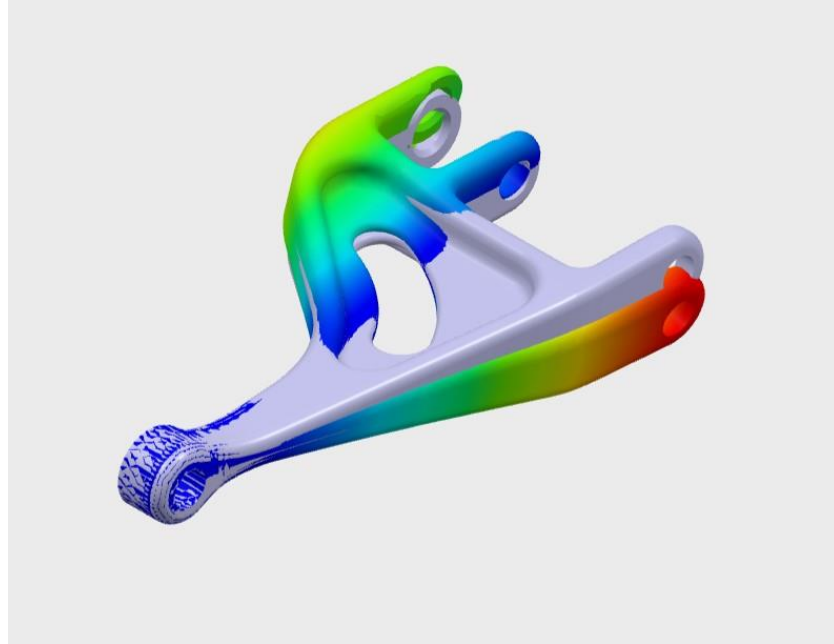


Figure 3.5. Original image and deformed image of the simulated part in the pre-processing stage.

3.3. ABAQUS/EXPLICIT

Abaqus/Explicit is an explicit-dynamic FEM solver of that is famous for electronic drop tests, ballistic impacts, automotive crash tests. Crash tests are divided into three main parts.

3.3.1. Structural Crashworthiness

It is used to find out the stress, displacement or energy absorption ability of a mechanical part caused by a vehicle hitting another stationary or moving vehicle. Frontal crash, rear crash, side crash, pole crash, rollover crash, etc. are some of the applications. The mechanical component is called crashworthy if it meets the required energy targets.



Figure 3.6. Abaqus/Explicit crash simulation of a car.

3.3.2. Drop Test

It is used to perform the free fall test of a particular object. Mobile phone, TV, airplane drop tests are some of its applications.

3.3.3. Passenger Safety

It simulates the impact of the accident on the driver and passengers in the vehicle. During the simulation, virtual mannequins called dummy are used.

3.4. CRASH BOX THEORETICAL FORMULAS

There are certain formulas when calculating crash tests and calculations are made based on these formulas [59–63]. These formulas are;

- Energy absorption (EA)
- Specific energy absorption (SEA)
- Mean crashing force (F_{avg})
- Crash force efficiency (CFE)
- Peak crashing force (F_{max})

3.4.1. Energy Absorption (EA)

The absorbed energy of a mechanical part exposed to axial crushing is formulated by integrating impact force F with respect to displacement x . Total absorbed energy is calculated as the area under the displacement-force curve of the crushing.

$$EA(d) = \int_0^d F(x)dx \quad (3.2)$$

d : crash displacement

F : axial impact force

3.4.2. Specific Energy Absorption (SEA)

SEA can be defined as absorbed energy per unit mass of the mechanical structure. In other words, SEA is defined as total absorbed energy divided by the mass of crash box tube.

$$SEA(d) = \frac{EA(d)}{mass (kg)} \quad (3.3)$$

3.4.3. Mean Crashing Force (F_{avg})

Mean crashing force is defined as total absorbed energy (EA) divided by crashing displacement.

$$F_{avg}(d) = \frac{EA(d)}{x} \quad (3.4)$$

3.4.4. Crash force efficiency (CFE)

CFE is defined as F_{avg} is divided by F_{max} .

$$CFE = \frac{F_{avg}(d)}{F_{max}} \quad (3.5)$$

Fmax: Maximum impact force

3.5. UNITS

There is no unit selection in ABAQUS, values must be entered according to the units given in the table below.

Table 3.2. Units of Abaqus software.

Quantity	SI	SI (mm)
Length	m	mm
Force	N	N
Mass	kg	Tonne (10 ³ kg)
Time	s	s
Stress	Pa (N/m ²)	MPa (N/mm ²)
Energy	J	mJ
Density	kg/m ³)	tonne/mm ³

3.6. MATERIAL

Many various materials have been used in studies for FCS [64–71]. The importance of aluminum and its alloys has also been emphasized by research [72]. The aluminum alloy 6000 series is used in this thesis.

3.6.1. Importance of Aluminum Alloy AA6061-T4

Aluminum and its alloys are lightweight materials [73]. This alloy has good high-strength properties. At the same time, it has excellent corrosion resistance, weldability, and machinability. AA6061 is the most popular aluminum extrusion.

3.6.1.1. Chemical components of aluminum alloy AA6061-T4

Stress-strain curves of AA6061-T4 studied before [74]. 95.9% of the weight of AA6061-T4 consists of aluminum. Other components are;

Table 3.3. Chemical components percentage in weight of AA6061-T4.

Elements	% in Weight
Magnesium (Mg)	1.2
Silicon (Si)	0.8
Iron (Fe)	0.7
Copper (Cu)	0.4
Chromium (Cr)	0.35
Zinc (Zn)	0.25
Manganese (Mn)	0.15
Titanium (Ti)	0.15
Other Elements	0.1

3.6.2. Properties of AA6061-T4

To run explicit simulations using the FEM method, the physical, mechanical and thermal properties of the AA6061-T4 material must be known. Such numerical properties are determined by tests such as tensile/compression.

3.6.2.1. Mechanical properties of AA6061-T4

Table 3.4. Mechanical properties of AA6061-T4.

Property	Value
Tensile Strength	241 MPa
Yield Strength	145 MPa
Modulus of Elasticity	68.9 GPa
Poisson's Ratio	0.33

3.6.2.2. Physical properties of AA6061-T4

Table 3.5. Physical properties of AA6061-T4.

Property	Value
Density	2.7 g/cm ³ (2.7e-9 t/mm ³)

3.6.2.3. Thermal properties of AA6061-T4

Table 3.6. Thermal properties of AA6061-T4.

Property	Value
Thermal Expansion (btw. 20 ⁰ -10 ⁰)	24 μm/m-K
Thermal Conductivity	170 W/m-K

PART 4

CRASH TESTS AND COMPARISON WITH FEM

THIN-WALLED CRASH TUBES

In this section, three different crash boxes with rectangular, circular and hexagonal cross sections are analyzed.

4.1. SINGLE CELL CRASH TUBES

4.1.1. Single-cell rectangular tube (SCR)

The crash tube was designed in the CATIA software and then Dynamic/Explicit analysis was performed using the finite element method with the ABAQUS software.

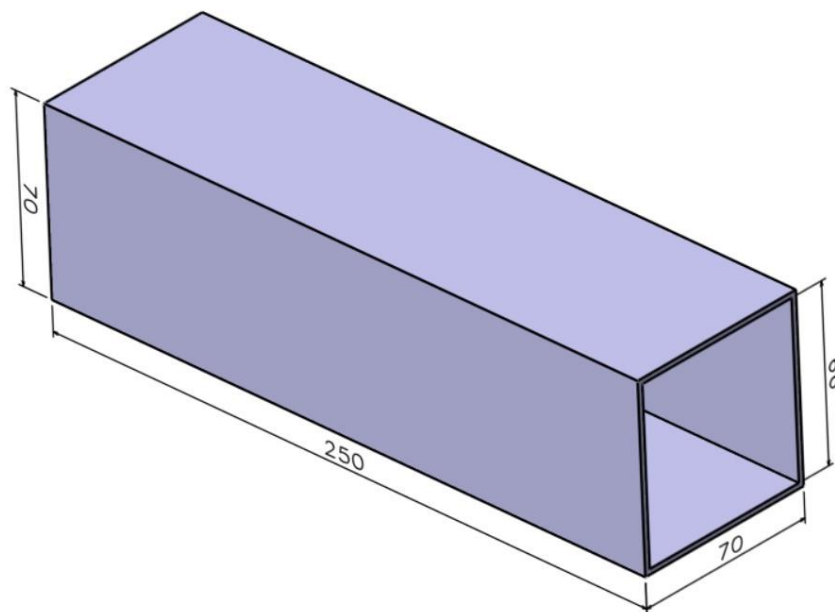


Figure 4.1. Rectangular cross-section crash box.

4.1.1.1. Simulation conditions of SCR

In the dynamic simulation, the tube hits a 50 kg wall with a speed of 43.2 km/h. The kinetic energy released by the impact is intended to be absorbed by the tube.

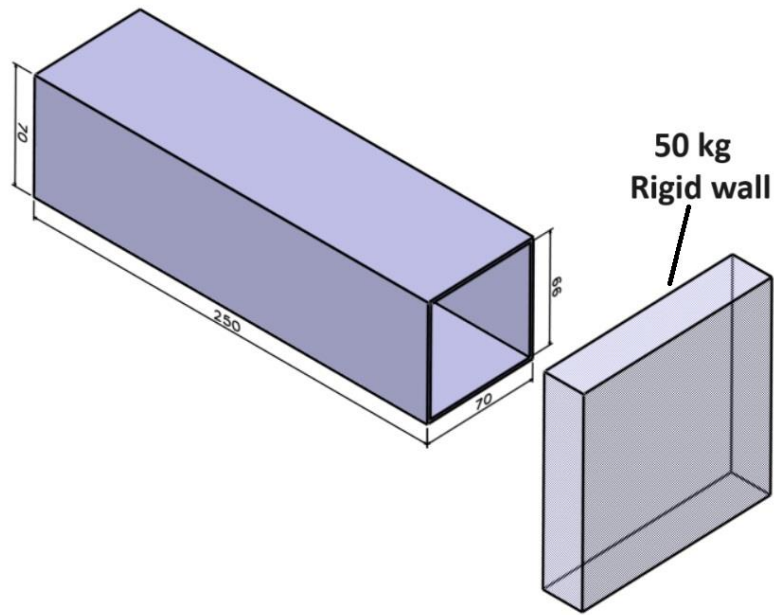


Figure 4.2. SCR and rigid wall representation.

Table 4.1. Simulation conditions of SCR.

Specifications of tube	Value
Height (mm)	70
Width (mm)	70
Length (mm)	250
Material	AA6061-T4
Wall thickness (mm)	2
Impact velocity (km/h)	43.2
Rigid wall mass (kg)	50

4.1.1.2. Dynamic simulation results of the SCR

Figure 4.3. shows how SCR subjected to an axial collision fold over time.

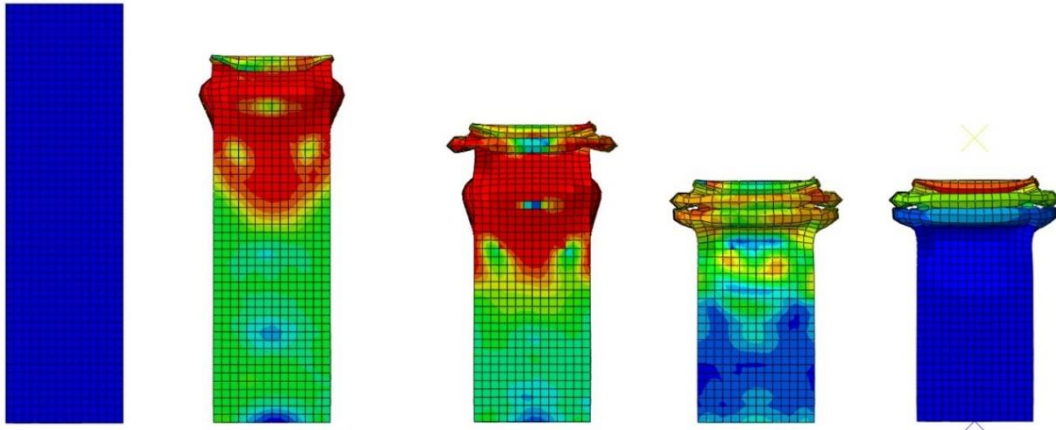


Figure 4.3. Folding process of SCR.

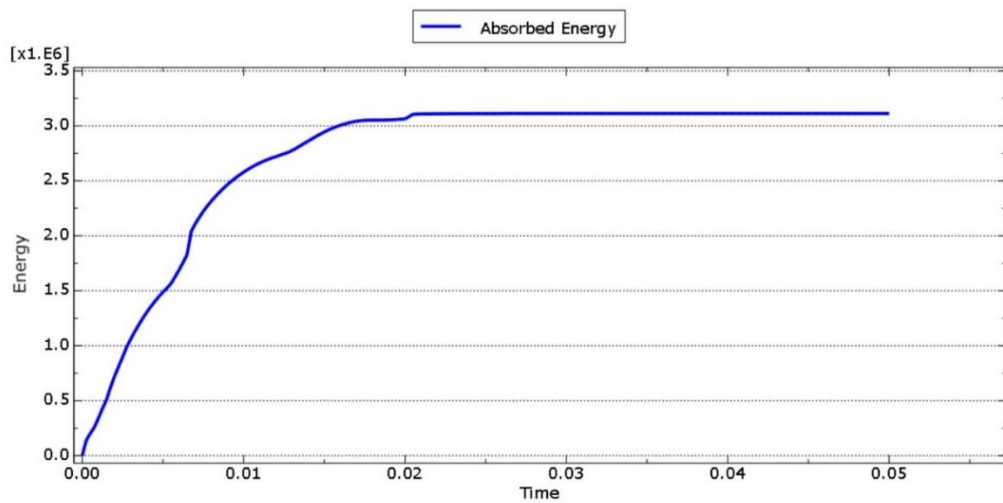


Figure 4.4. Absorbed energy during the crash of SCR.

Above Figure 4.4. shows that the tube absorbs the kinetic energy generated at the moment of impact. The tube folds and absorbs the kinetic energy generated during the crash. When the crash ends, the kinetic energy also ends, and as can be seen in the graph, there is no increase in the absorbed kinetic energy, the graph remains constant. The crash tubes and bumper beam are folding and absorb the kinetic energy generated during the accident. If the tube and beam mechanisms cannot absorb kinetic energy, the kinetic energy is transferred to the vehicle and the vehicle is damaged.

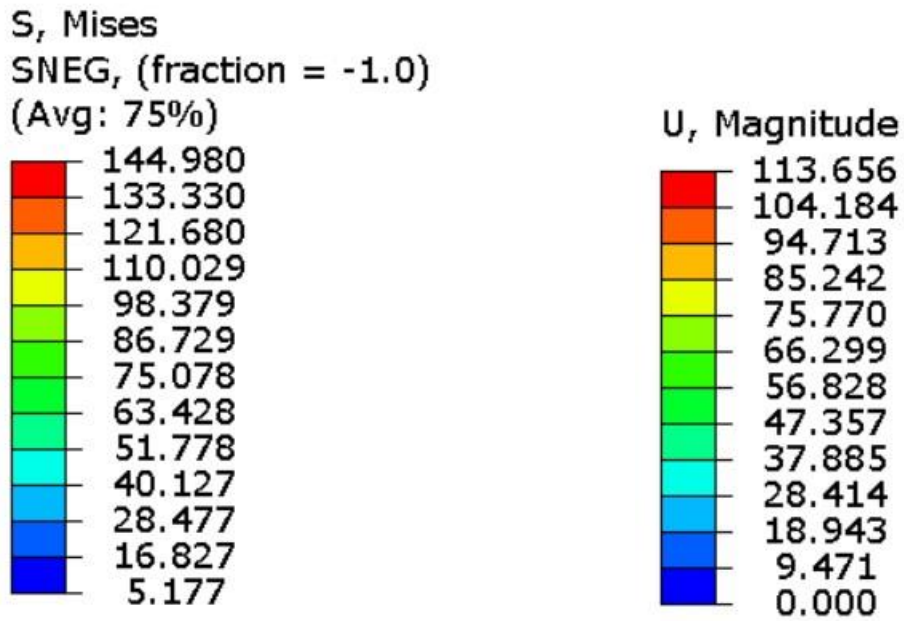


Figure 4.5. Von misses (left) and displacement (right) of SCR.

Table 4.2. Simulation results of SCR.

Result	Value
Mass (kg)	0.376
AE (J)	3112.5
SEA (J/kg)	8277.9
Fmax kN	38.448
Von mises (MPa)	144.980
Displacement (mm)	113.656

4.1.2. Single-cell circular tube (SCC)

The circular section tube was also tested under the same analysis conditions as the rectangular one whose analysis results are given above.

4.1.2.1 Simulation conditions of SCC

In the dynamic simulation, the tube hits a 50 kg wall with a speed of 43.2 km/h. The kinetic energy released by the impact is intended to be absorbed by the tube.

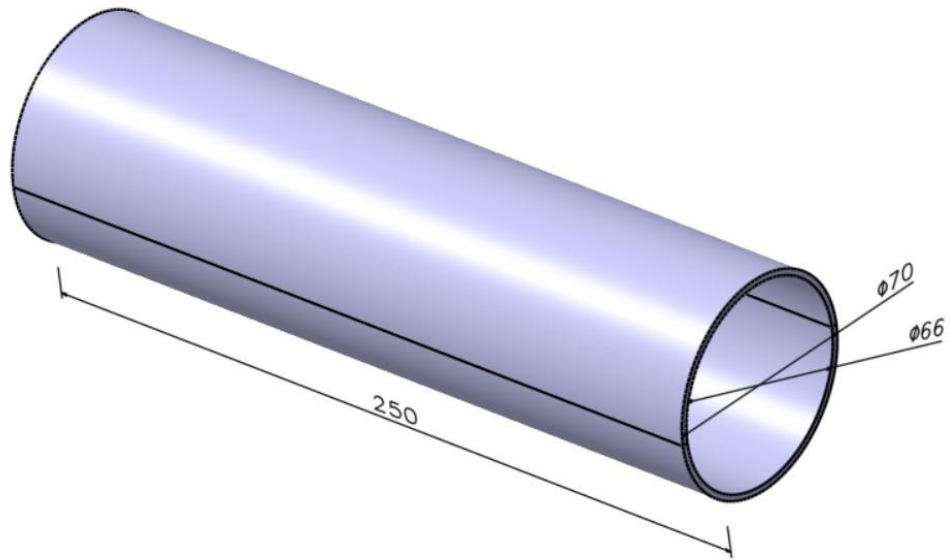


Figure 4.6. Circular cross-section crash box representation.

Table 4.3. Simulation conditions of SCC.

Specifications of tube	Value
Diameter (mm)	70
Length (mm)	250
Material	AA6061-T4
Wall thickness (mm)	2
Impact velocity (km/h)	43.2
Rigid wall mass (kg)	50

4.1.2.2. Dynamic simulation results of the SCC

Figure 4.7. shows how SCC subjected to an axial collision fold over time.

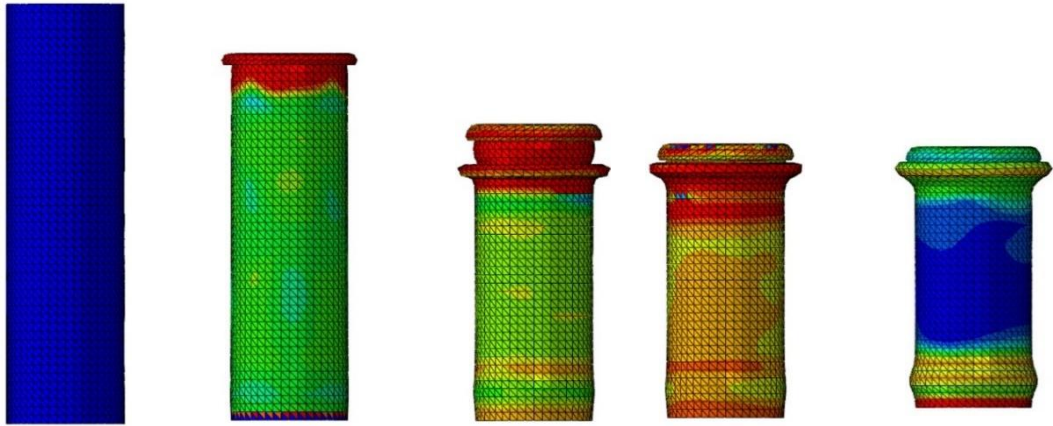


Figure 4.7. Folding process of SCC.

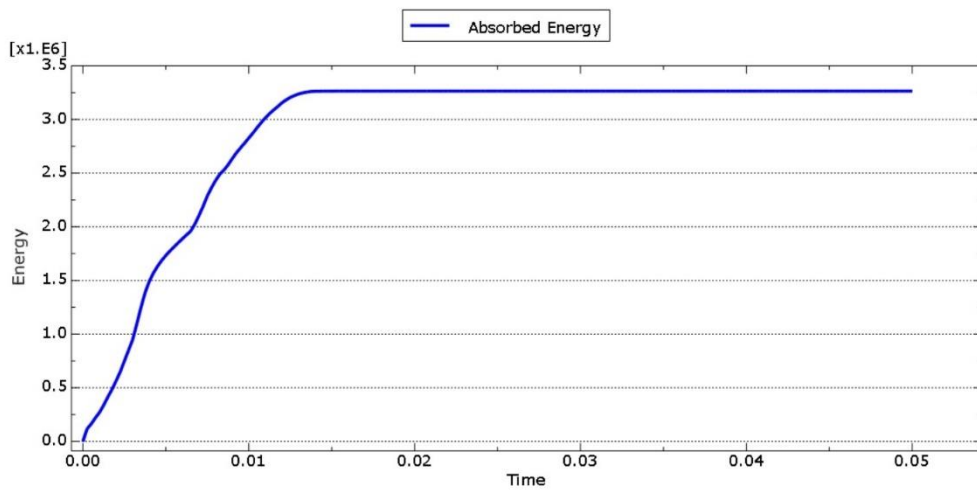


Figure 4.8. Absorbed energy during the crash of SCC.

The same graph emerged in the circular cross-section sample as in the rectangular cross-section sample. The total absorbed energy by SCC is 3263.7 J. Thus, it was observed that SCC absorbed more energy than SCR under the same conditions.

Von mises stress value for SCC is 144.189 MPa which is almost the same with the SCR. Total displacement is 98.945 that is lower than SCR.

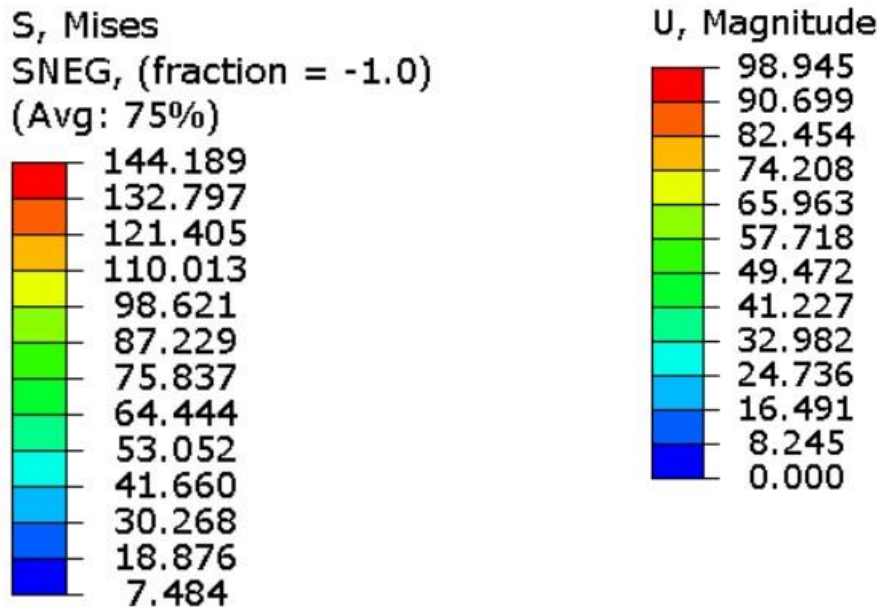


Figure 4.9. Von misses (left) and displacement (right) of SCC.

Table 4.4. Simulation results of SCC.

Result	Value
Mass (kg)	0.288
AE (J)	3263.7
SEA (J/kg)	11332.3
Fmax kN	45.442
Von mises (MPa)	144.189
Displacement (mm)	98.945

4.1.3. Single-cell hexagonal tube (SCH)

In this section, the hexagonal cross section tube was simulated under the same conditions as the studies whose results were given above.

4.1.3.1. Simulation conditions of SCH

In the dynamic simulation, the tube hits a 50 kg wall with a speed of 43.2 km/h. The kinetic energy released by the impact is intended to be absorbed by the tube.

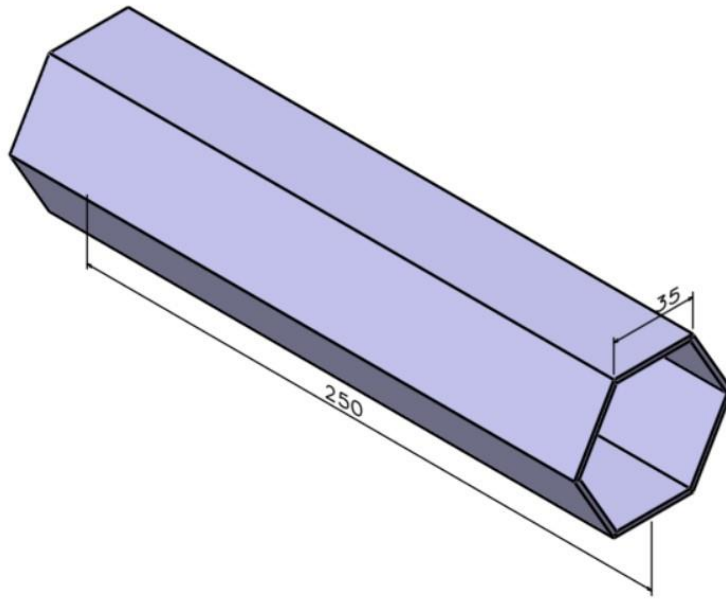


Figure 4.10. Hexagonal cross-section crash box representation.

Table 4.5. Simulation conditions of SCH.

Specifications of tube	Value
Width (mm)	70
Length (mm)	250
Material	AA6061-T4
Wall thickness (mm)	2
Impact velocity (km/h)	43.2
Rigid wall mass (kg)	50

4.1.3.2. Dynamic simulation results of the SCH

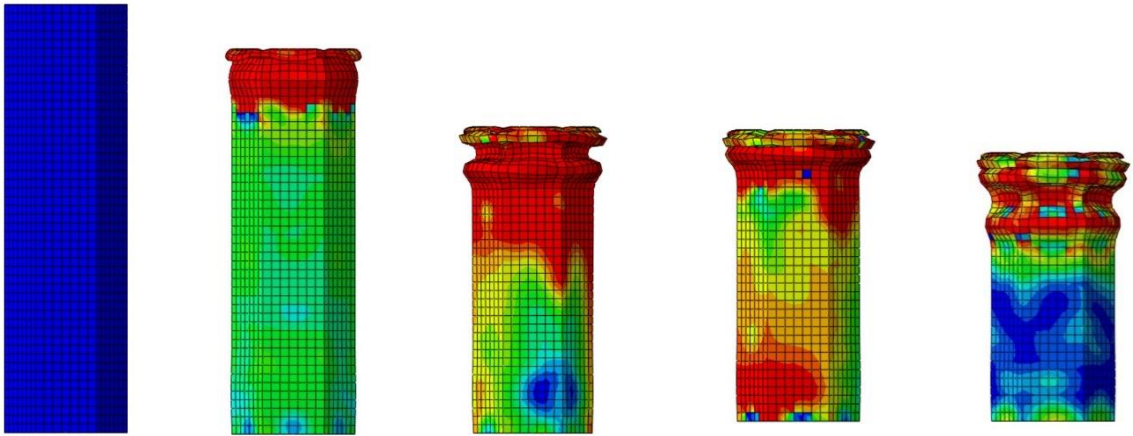


Figure 4.11. Folding process of SCH.

Figure 4.11. shows how SCH subjected to an axial collision fold over time.

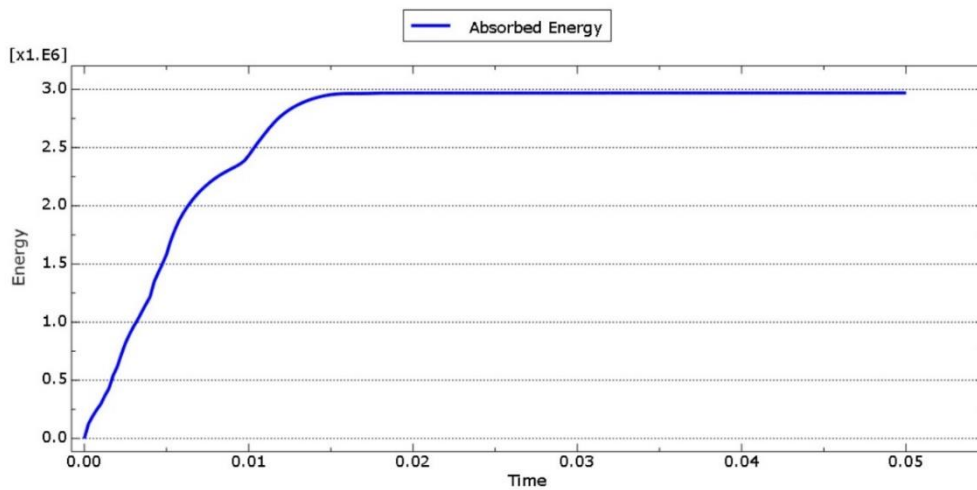


Figure 4.12. Absorbed energy during the crash of SCH.

The same graph emerged in the hexagonal cross-section samples as in the rectangular and circular cross-section sample. The total absorbed energy by SCH is 2970.2 J. Thus, it was observed that SCH absorbed less energy than SCR & 2 under the same conditions.

Von mises stress value for SCH is 145 MPa which is almost the same with the SCR & 2. Total displacement is 96.945 that is lower than SCR & 2.

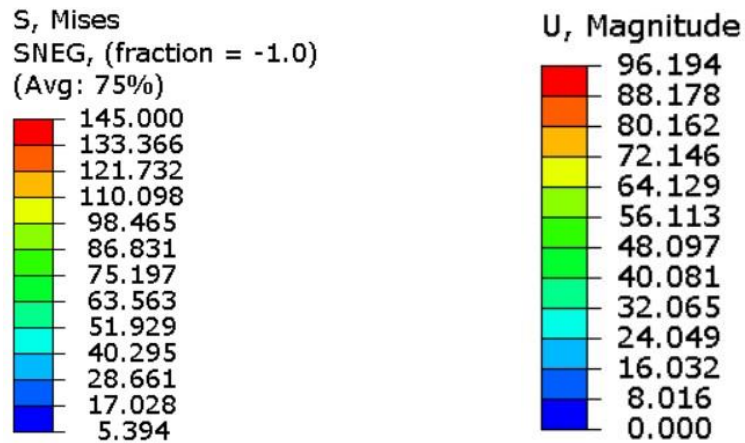


Figure 4.13. Von misses (left) and displacement (right) of SCH.

Table 4.6. Simulation results of SCH.

Result	Value
Mass (kg)	0.274
AE (J)	2970.2
SEA (J/kg)	10839.4
Fmax kN	34.449
Von mises (MPa)	145
Displacement (mm)	96.194

4.2. MULTI-CELL CRASH TUBES

4.2.1. Multi-cell rectangular tube (MCR)

In this section, unlike the first section, crash tubes consisting of multiple cell structures were analyzed.

4.2.1.1. Simulation conditions of MCR

In the dynamic simulation, the tube hits a 50 kg wall with a speed of 43.2 km/h. The kinetic energy released by the impact is intended to be absorbed by the tube.

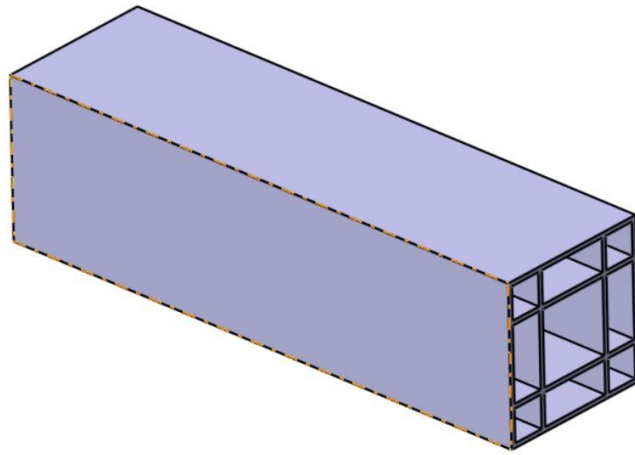


Figure 4.14. Rectangular multi-cell cross-section crash box.

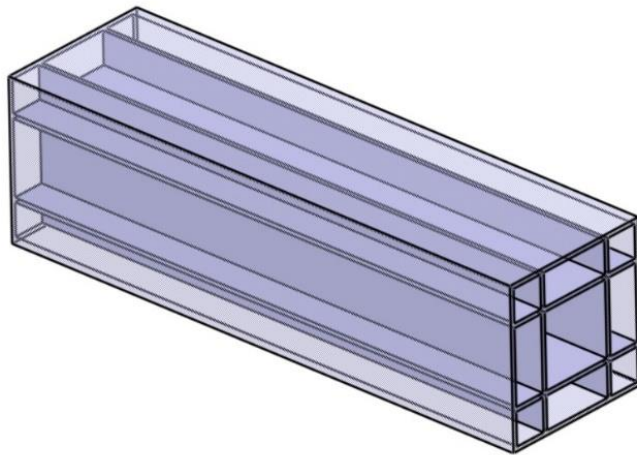


Figure 4.15. Transparent and FEM representation of MCR.

Table 4.7. Simulation conditions of MCR.

Specifications of tube	Value
Height (mm)	70
Width (mm)	70
Length (mm)	250
Material	AA6061-T4
Wall/cell thickness (mm)	2
Impact velocity (km/h)	43.2
Rigid wall mass (kg)	50

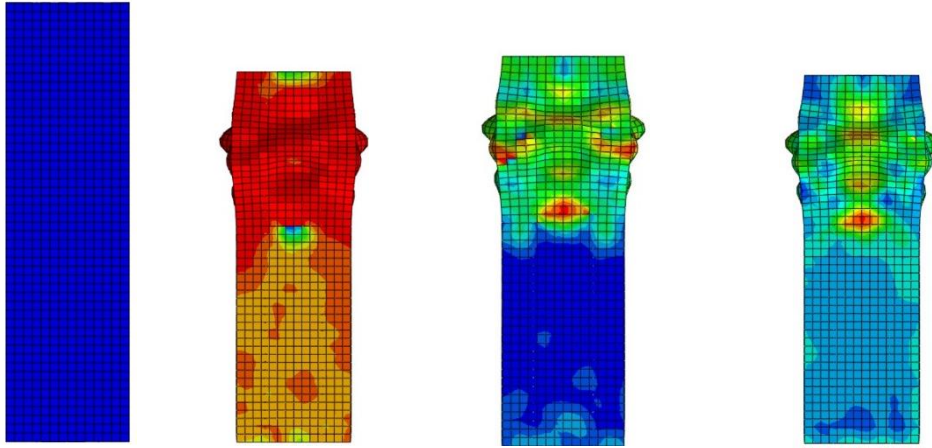


Figure 4.16. Folding process of MCR.

4.2.1.2. Dynamic simulation results of the MCR

Figure 4.16. shows how MCR subjected to an axial collision fold over time.

The same graph emerged in the previous samples as in the rectangular and hexagonal cross-section sample. (Fig. 4.17.)

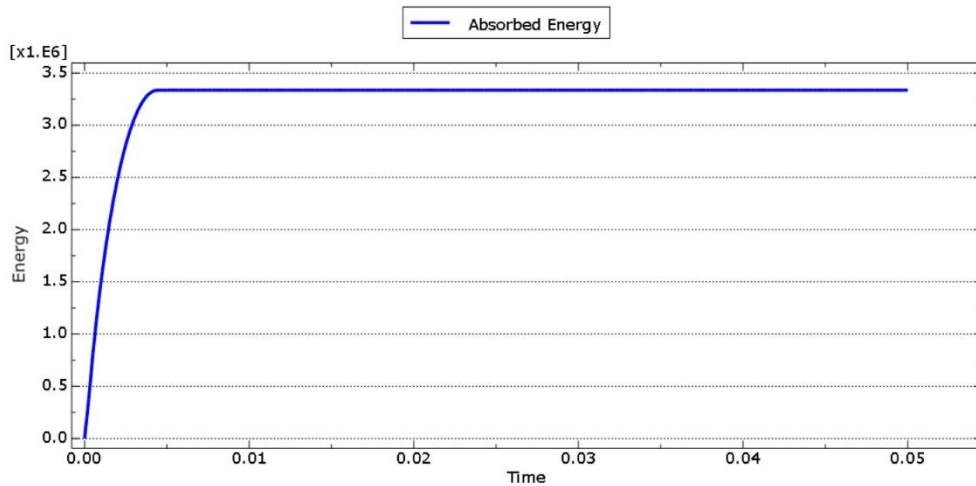


Figure 4.17. Absorbed energy during the crash of MCR.

The same graph emerged in the previous samples. The total absorbed energy by MCR is 3366.6 J. Thus, it was observed that MCR absorbed more energy among others.

Von mises stress value for MCR is 141.776 MPa. Total displacement is 27.409 that is lower than other tubes.

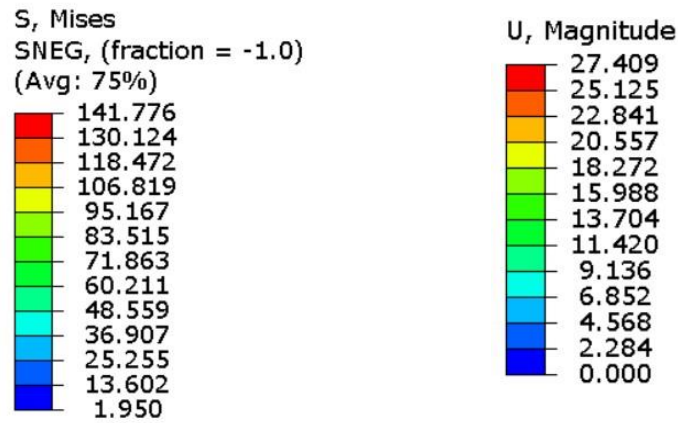


Figure 4.18. Von misses (left) and displacement (right) of MCR.

Table 4.8. Simulation results of MCR.

Result	Value
Mass (kg)	0.713
AE (J)	3366.6
SEA (J/kg)	4721.74
Fmax kN	34.851
Von mises (MPa)	141.776
Displacement (mm)	27.409

4.2.2. Multi-cell circular tube (MCC)

In the dynamic simulation, the multi-cell circular tube hits a 50 kg wall with a speed of 43.2 km/h. The kinetic energy released by the impact is intended to be absorbed by the tube.

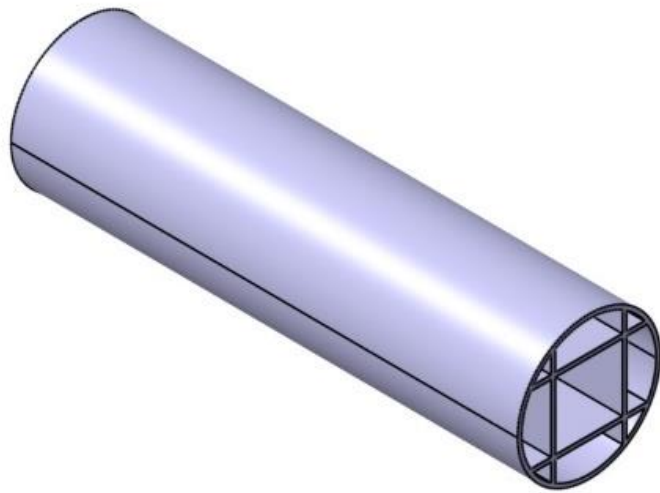


Figure 4.19. MCC representation

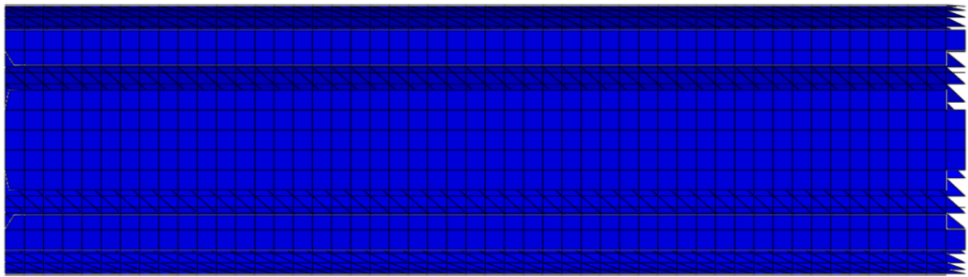


Figure 4.20. Sectioned view of MCC at time 0.

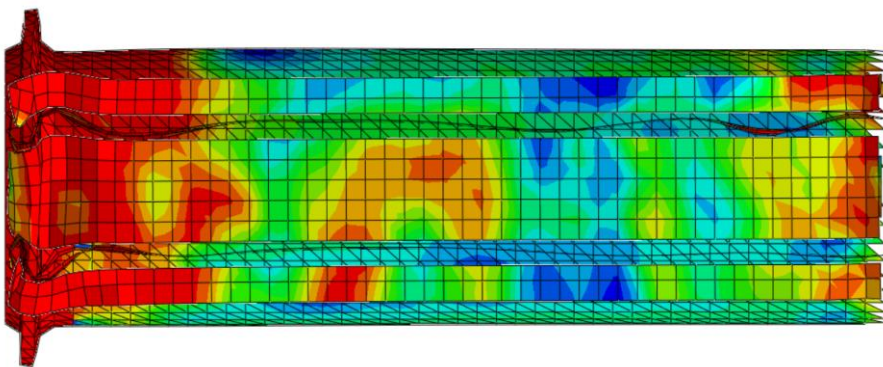


Figure 4.21. Sectioned view of MCC at first fold.

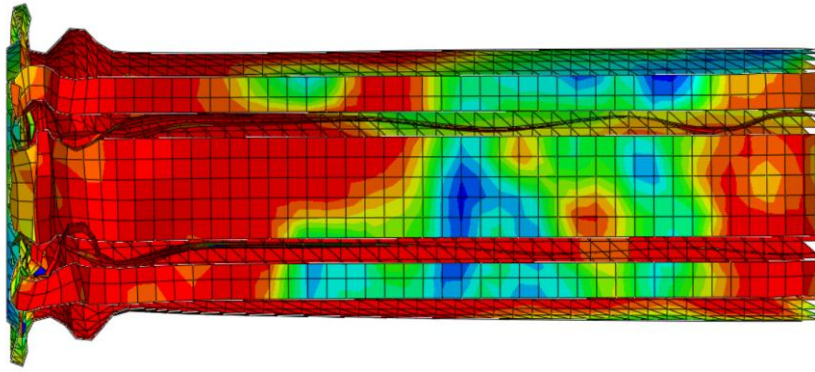


Figure 4.22. Sectioned view of MCC at second fold.

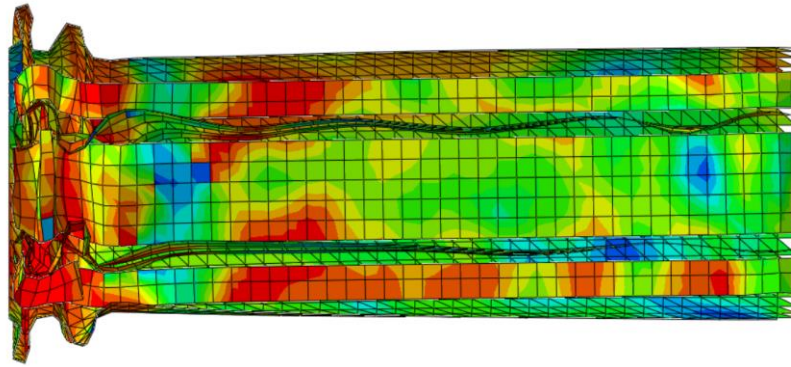


Figure 4.23. Sectioned view of MCC at the final.

4.2.2.1. Simulation conditions of MCC

Table 4.9. Simulation conditions of MCC.

Specifications of tube	Value
Diameter (mm)	70
Length (mm)	250
Material	AA6061-T4
Wall thickness (mm)	2
Impact velocity (km/h)	43.2
Rigid wall mass (kg)	50

4.2.2.2. Dynamic simulation results of the MCC

Table 4.10. Simulation results of MCC.

Result	Value
Mass (kg)	0.580
AE (J)	3070.7
SEA (J/kg)	5294.31
Fmax kN	66.264
Von mises (MPa)	143.902
Displacement (mm)	47.649

The total absorbed energy of MCC is 3070.7 J. Thus, it was observed that MCC absorbed average energy among others.

Von mises stress value for MCC is 143.902 MPa. Total displacement is 47.649 that is lower than other tubes.

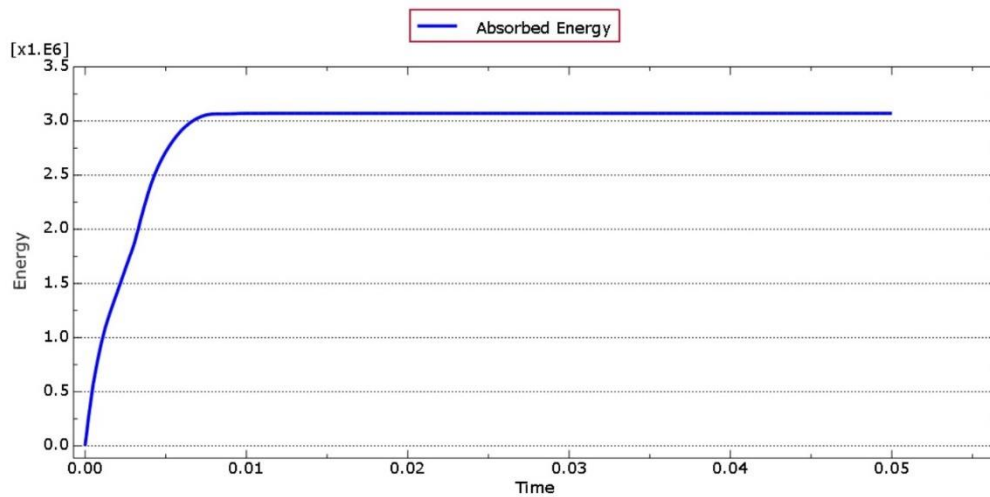


Figure 4.24. Absorbed energy during the crash of MCC.

4.3.1. Multi-cell hexagonal tube (MCH)

In the dynamic simulation, the multi-cell hexagonal tube hits a 50 kg wall with a speed of 43.2 km/h. The kinetic energy released by the impact is intended to be absorbed by the tube.

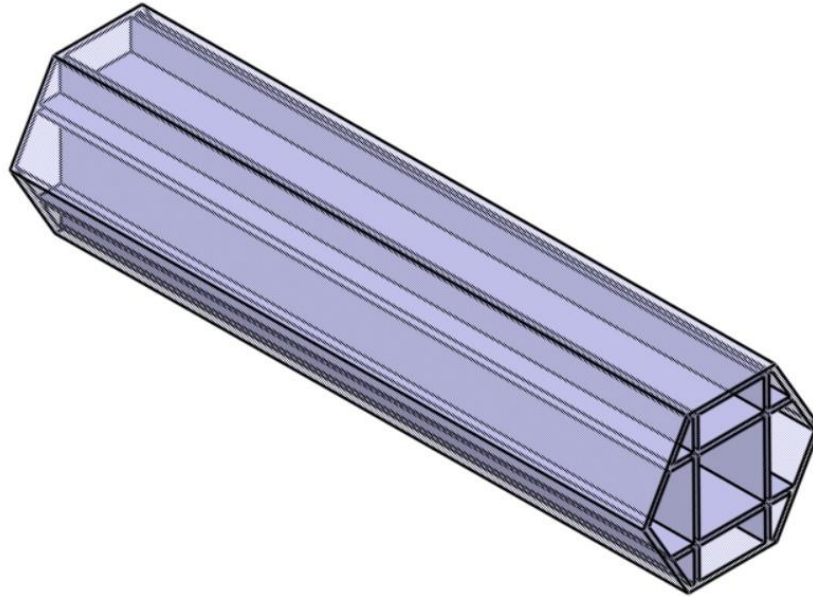


Figure 4.25. MCH representation.

4.3.1.1. Simulation conditions of MCH

Table 4.11. Simulation conditions of MCH

Specifications of tube	Value
Diameter (mm)	70
Length (mm)	250
Material	AA6061-T4
Wall thickness (mm)	2
Impact velocity (km/h)	43.2
Rigid wall mass (kg)	50

4.3.1.2. Dynamic simulation results of the MCH

Figure 4.26. shows how MCH subjected to an axial collision fold over time.

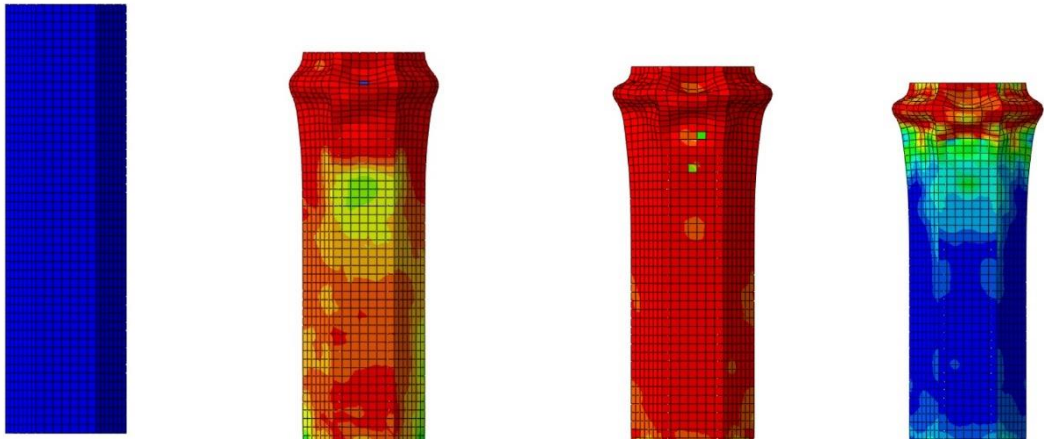


Figure 4.26. Folding process of the MCH.

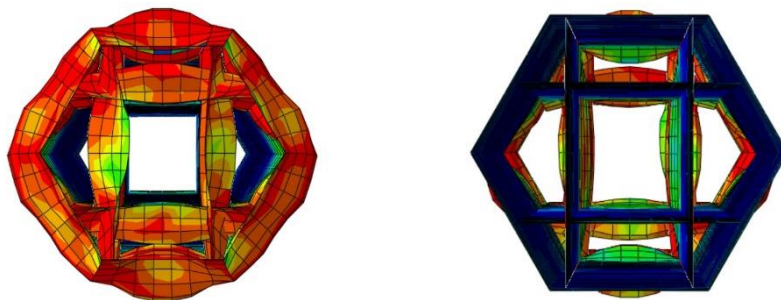


Figure 4.27. Axial folding process representation of the MCH.

Table 4.12. Simulation results of MCH.

Result	Value
Mass (kg)	0.544
AE (J)	3052.86
SEA (J/kg)	5611.88
Fmax kN	105.574
Von mises (MPa)	143.594
Displacement (mm)	33.352

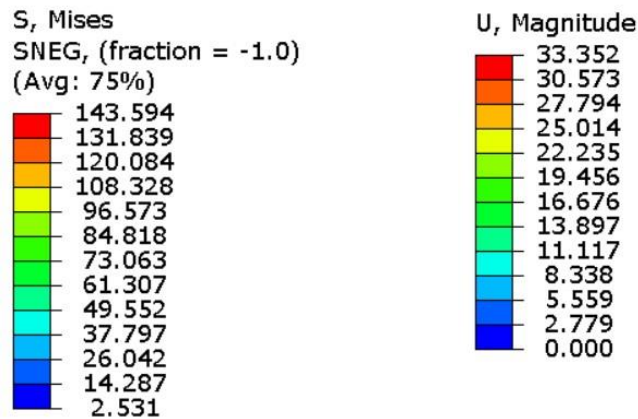


Figure 4.28. Von misses (left) and displacement (right) of MCH.

BUMPER BEAM

Honeycomb sandwich structures are used to add strength to structures through engineering studies. Honeycomb structures are also among the strongest structures in terms of strength to weight ratio [75].

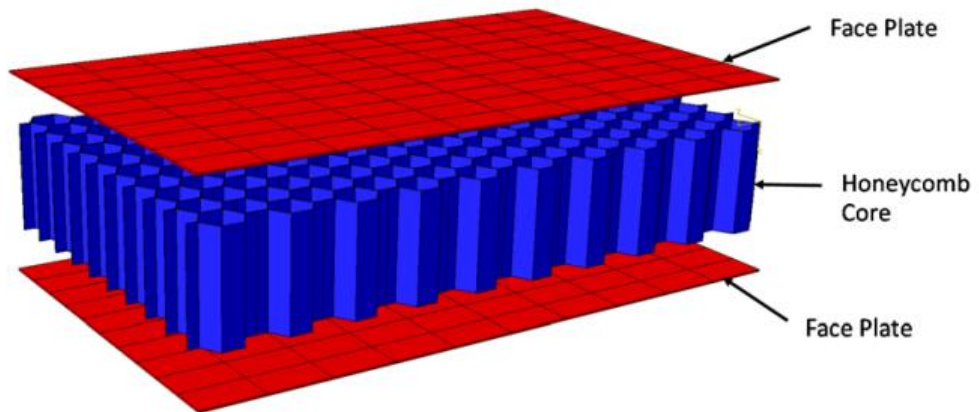


Figure 4.29. Sandwich composite structure [76].

Honeycomb structures are made from metallic materials as well as by 3D printing production [77]. Various studies have been carried out in terms of energy absorption of honeycomb structures [78,79]. Studies show that filling the bumper beam with a honeycomb structure made of aluminum or another material foam increases the energy absorption of the beam [80–86].

4.3. SINGLE-CELL BUMPER BEAM (SCB)

In this section, the simulation of the single-cell bumper beam under dynamic analysis conditions were carried out. Crash tubes were used in the beam simulation and thus it was observed how the FCS would behave at the time of crash.

In the simulation, a 50 kg rigid wall hit the FCS at a speed of 57.6 km/h in the axial direction, and the displacement and energy absorption of the system were calculated.

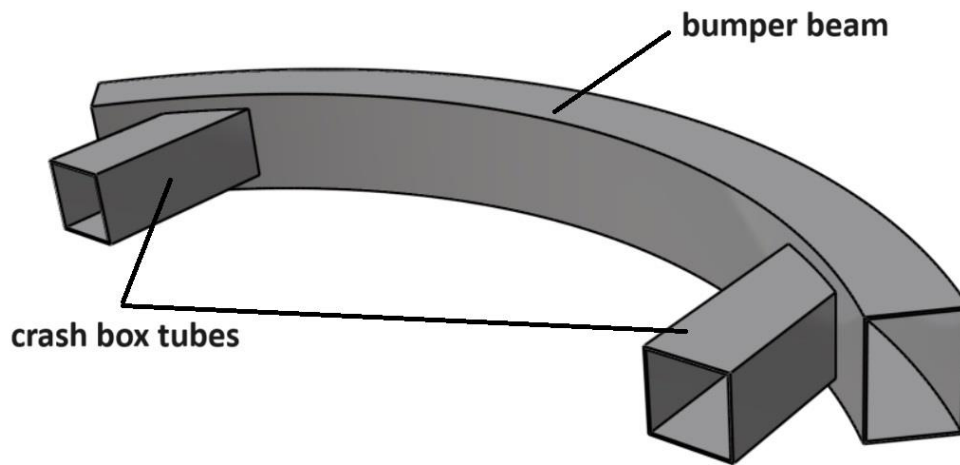


Figure 4.30. SCB representation.

4.3.1. Simulation conditions of SCB

Table 4.13. Simulation conditions of SCB.

Specifications of beam	Value
Height (mm)	70
Width (mm)	70
Material	AA6061-T4
Wall thickness (mm)	2
Impact velocity (km/h)	57.6
Rigid wall mass (kg)	50

4.3.2. Dynamic simulation results of the SCB

Table 4.14. Simulation results of SCB.

Result	Value
Mass (kg)	1.902
AE (J)	4012.88
SEA (J/kg)	2109.82
Fmax kN	25.575
Von mises (MPa)	133.648
Displacement (mm)	254.725

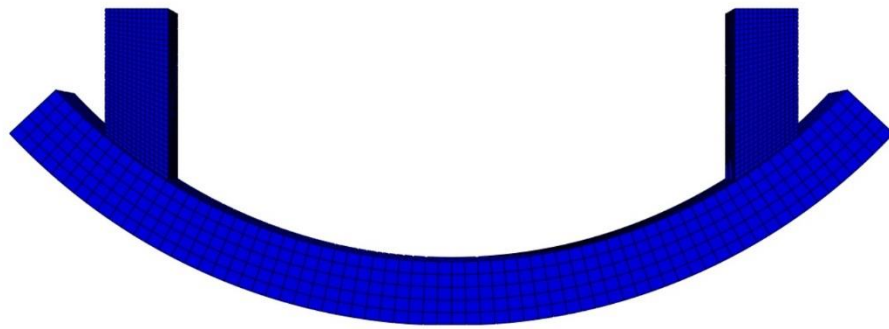


Figure 4.31. SCB initial representation

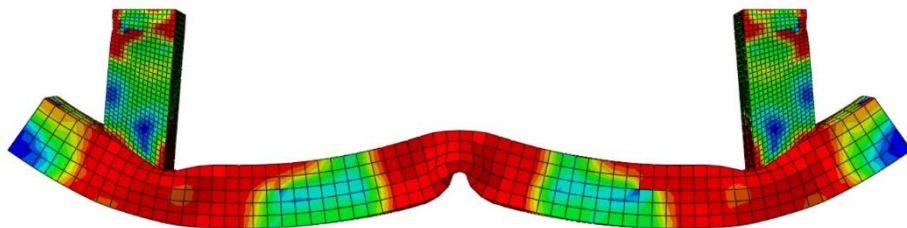


Figure 4.32. SCB crash representation at time 0.025 ms.

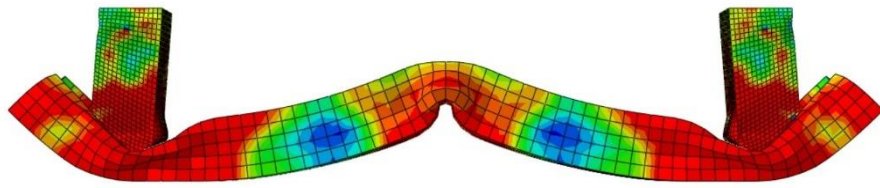


Figure 4.33. SCB crash representation at time 0.05 ms.

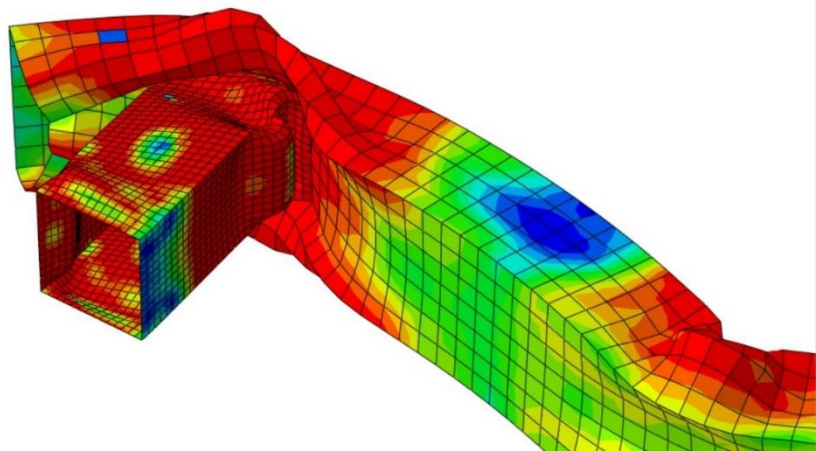


Figure 4.34. SCB crash box and beam representation at time 0.05 ms.

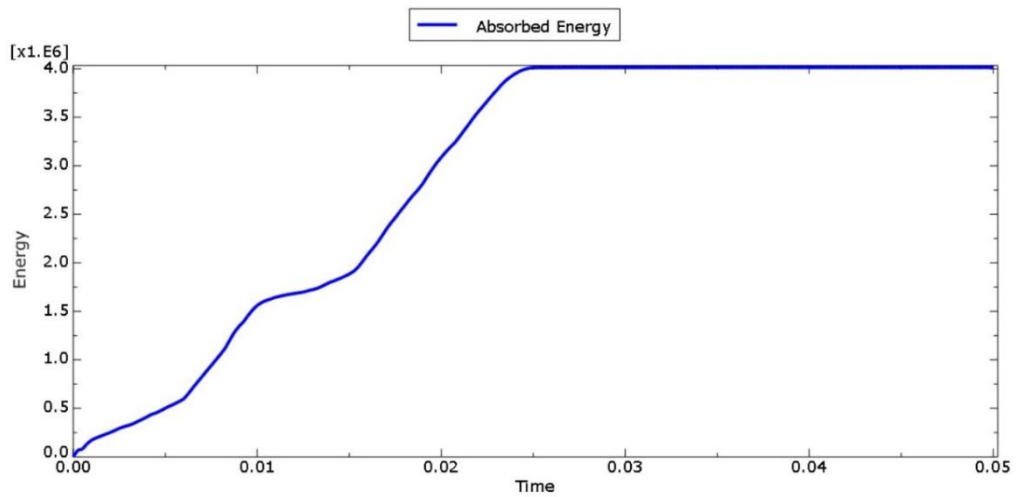


Figure 4.35. Absorbed energy of SCB.

4.4. MULTI-CELL BUMPER BEAM (MCB)

In this section, the simulation of the multi-cell bumper beam under dynamic analysis conditions were carried out. Crash tubes were used in the beam simulation and thus it was observed how the FCS would behave at the time of crash.

In the simulation, a 50 kg rigid wall hit the FCS at a speed of 57.6 km/h in the axial direction, and the displacement and energy absorption of the system were calculated.

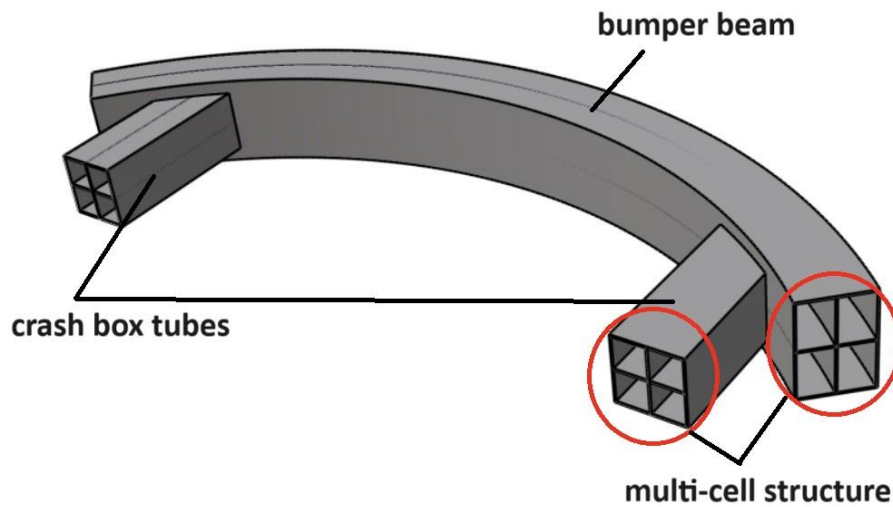


Figure 4.36. MCB representation.

4.3.1. Simulation conditions of MCB

Table 4.15. Simulation conditions of MCB.

Specifications of beam	Value
Height (mm)	70
Width (mm)	70
Material	AA6061-T4
Wall thickness (mm)	2
Cell thickness (mm)	2
Impact velocity (km/h)	57.6
Rigid wall mass (kg)	50

4.3.2. Dynamic simulation results of the MCB

Table 4.16. Simulation results of MCB.

Result	Value
Mass (kg)	2.820
AE (J)	5221.08
SEA (J/kg)	1851.44
Fmax kN	34.884
Von mises (MPa)	143.524
Displacement (mm)	216.931

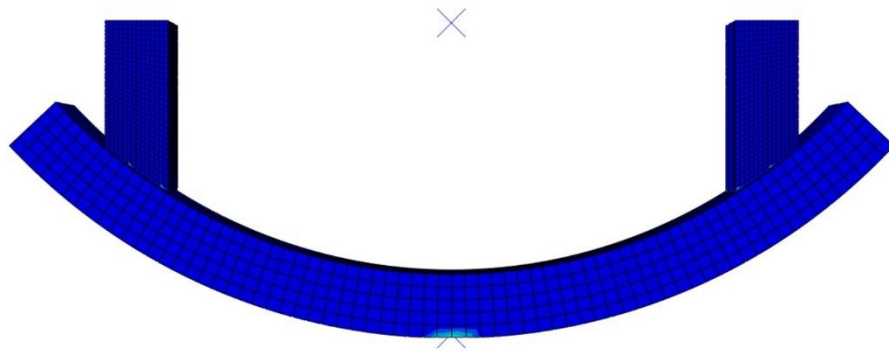


Figure 4.37. MCB initial representation

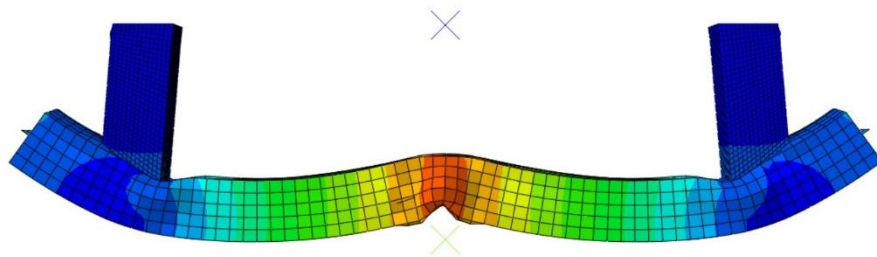


Figure 4.38. MCB crash representation at time 0.025 ms.

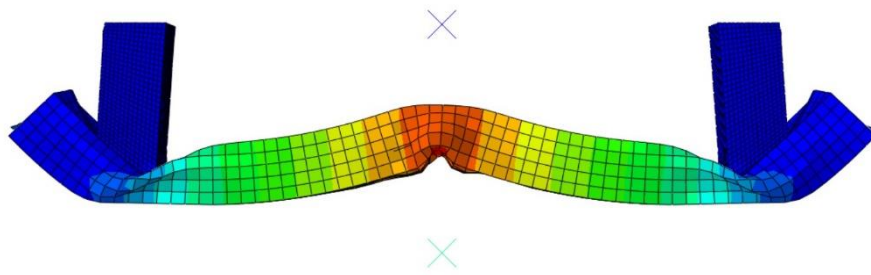


Figure 4.39. MCB crash representation at time 0.05 ms.

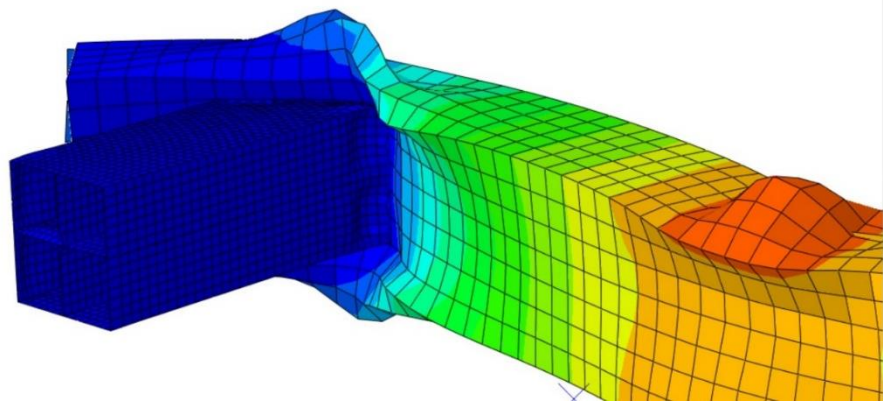


Figure 4.40. MCB crash box and beam representation at time 0.05 ms.

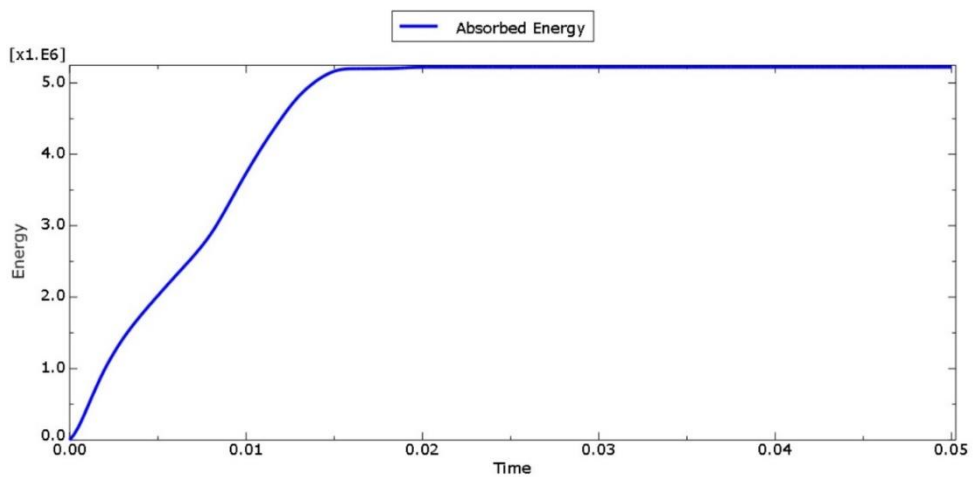


Figure 4.41. Absorbed energy of MCB.

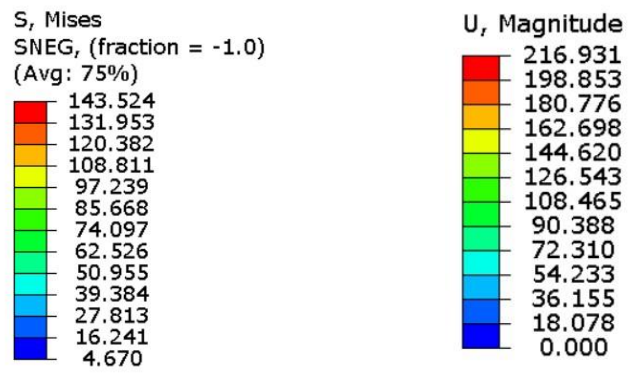
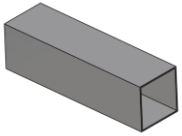
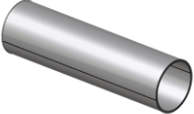
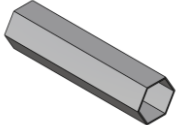
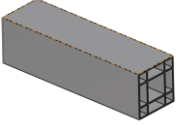
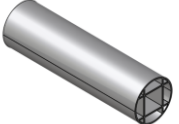
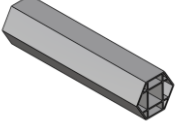
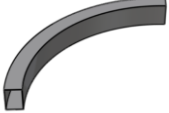


Figure 4.42. Von Misses (left) and displacement (right) values of MCB.

PART 5

RESULTS AND DISCUSSION

Table 5.1. Crash Box tubes and bumper beams representations.

Crash Box Tubes and Bumper Beams		
Name	Code	Representation
Single-cell rectangular	SCR	
Single-cell circular	SCC	
Single-cell hexagonal	SCH	
Multi-cell rectangular	MCR	
Multi-cell circular	MCC	
Multi-cell hexagonal	MCH	
Single-cell bumper beam	SCB	

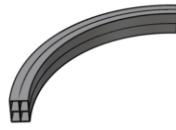
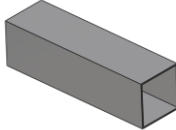
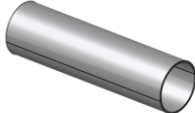
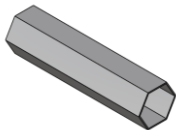
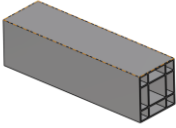
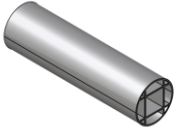
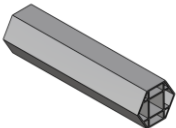
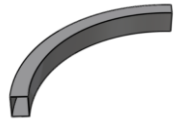
Multi-cell bumper beam	MCB	
------------------------	-----	---

Table 5.2. Simulation Results-I.

Crash Box Tubes and Bumper Beams		
Simulation Results-I		Representation
Mass (kg)	0.376	
Von misses (MPa)	144.980	
Displacement (mm)	113.656	
Mass (kg)	0.288	
Von misses (MPa)	144.189	
Displacement (mm)	98.945	
Mass (kg)	0.274	
Von misses (MPa)	145	
Displacement (mm)	96.167	
Mass (kg)	0.713	
Von misses (MPa)	141.776	
Displacement (mm)	27.409	
Mass (kg)	0.580	
Von misses (MPa)	143.902	
Displacement (mm)	47.649	
Mass (kg)	0.544	
Von misses (MPa)	143.594	
Displacement (mm)	33.352	
Mass (kg)	1.902	
Von misses (MPa)	133.648	
Displacement (mm)	254.725	
Mass (kg)	2.820	
Von misses (MPa)	143.524	

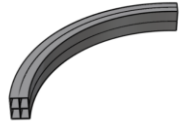
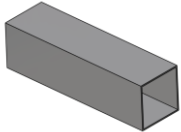

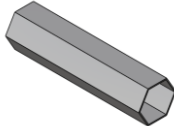
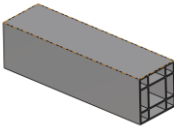
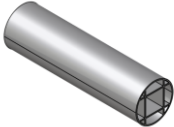
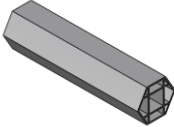

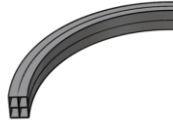
Displacement (mm)	216.931	
-------------------	---------	---

Table 5.3. Simulation Results-II.

Crash Box Tubes and Bumper Beams		
Simulation Results-II		Representation
Energy Absorption (J)	3112.5	
Specific Energy Absorption (J/kg)	8277.9	
Fmax (N)	38.448	
Energy Absorption (J)	3263.7	
Specific Energy Absorption (J/kg)	11332.3	
Fmax (N)	45.442	
Energy Absorption (J)	2970.2	
Specific Energy Absorption (J/kg)	10839.4	
Fmax (N)	34.449	
Energy Absorption (J)	3366.6	
Specific Energy Absorption (J/kg)	4721.7	
Fmax (N)	34.851	
Energy Absorption (J)	3070.7	
Specific Energy Absorption (J/kg)	5294.3	
Fmax (N)	66.264	
Energy Absorption (J)	3052.86	
Specific Energy Absorption (J/kg)	5611.88	

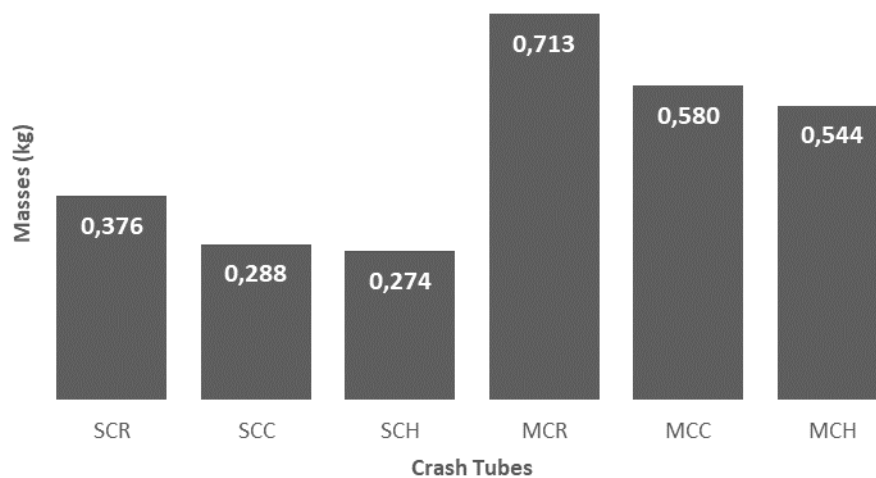
Fmax (N)	105.574	
Energy Absorption (J)	4012.88	
Specific Energy Absorption (J/kg)	2109.82	
Fmax (N)	25.575	
Energy Absorption (J)	5221.08	
Specific Energy Absorption (J/kg)	1851.44	
Fmax (N)	34.884	

5.1. WEIGHT COMPARISON

When we compare single-cell boxes in terms of weight, the rectangular section tube is the heaviest. Tubes with circular and hexagonal cross-sections come respectively.

When we compare multi-cell boxes in terms of weight, they are ranked from heaviest to lightest, respectively, with rectangular cross-section, circular and hexagonal cross-section tubes.

Table 5.4. Mass comparison of tubes.

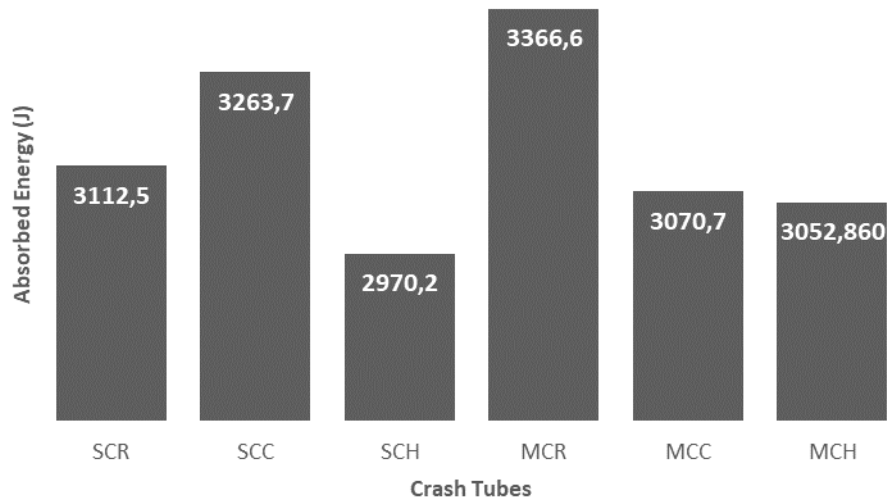


5.2. ENERGY ABSORPTION COMPARISON

In single-cell tubes, the circular cross-section tube has the highest energy absorption. The circular tube is followed by rectangular and hexagonal tubes, respectively.

When we compare multi-cell boxes in terms of energy absorption, they are ranked from rectangular cross-section, circular and hexagonal cross-section tubes.

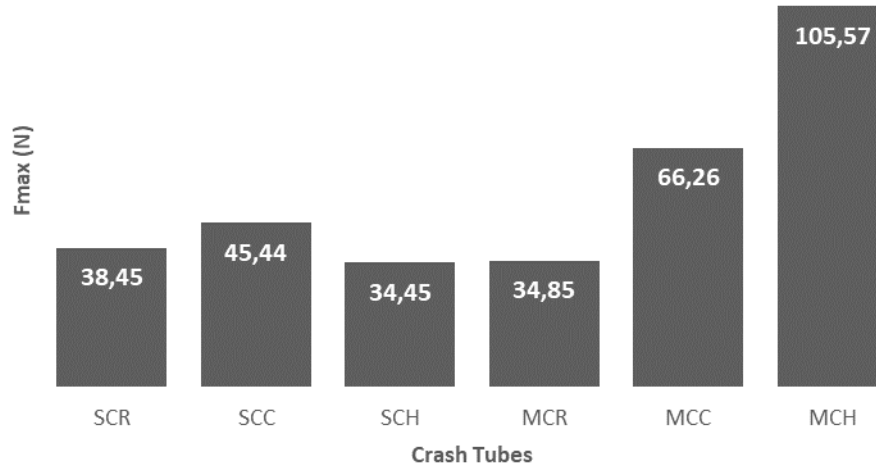
Table 5.5. Energy absorption comparison of tubes.



5.3. MAXIMUM IMPACT FORCE

Fmax is another important criteria for the crash box tube. The lower the Fmax, the easier it is to fold the tube. If a high force occurs, the tube cannot be folded to absorb energy and all the energy is transferred to the vehicle.

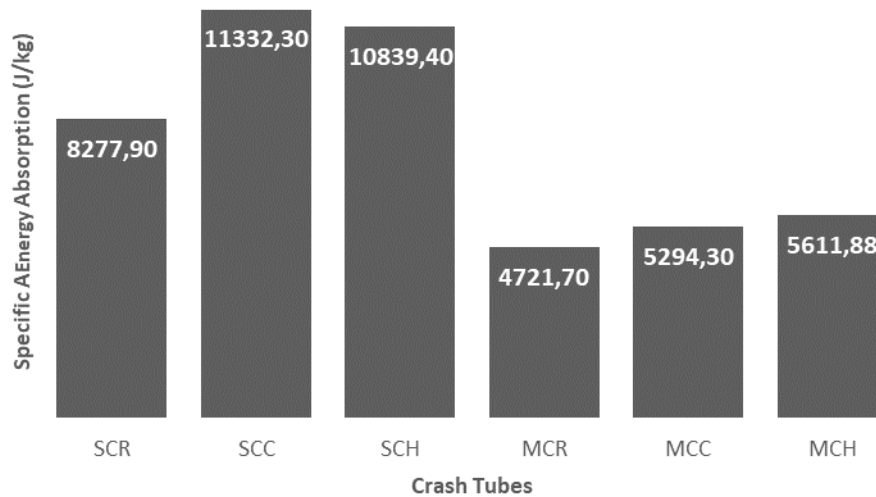
Table 5.6. Fmax comparison of tubes.



5.4. SPECIFIC ENERGY ABSORPTION

This parameter is found by dividing the energy absorbed by the tube by its mass. It is used to find the energy absorbed per mass.

Table 5.7. SEA comparison of tubes.



PART 6

CONCLUSION

In this study, dynamic/explicit analyses of crash box tubes and bumper beams were performed in terms of strength/weight ratio.

- When we evaluate in terms of mass, multicellular crash box tubes are naturally heavier because they contain axial cells. In both multi-cell and single-cell tubes, rectangular section tubes are heavier than other tubes.
- When we evaluate it in terms of absorbed energy, the multi-cell rectangular section tube absorbed the most energy. Since multi-cell circular and hexagonal cross-section tubes folded less than rectangular cross-section tubes at the time of collision, they could not absorb enough energy. For this reason, they are more likely to transmit the kinetic energy generated in the event of a collision to the vehicle.
- The maximum force (F_{max}) generated at the moment of first collision is one of the most important parameters for us. In order for a tube to absorb energy in the event of an accident, it must be folded properly. The higher the F_{max} at the time of the accident, the more difficult it is to fold the tubes. For this reason, multi-cell rectangular section tube should be preferred due to the high absorbed energy and low F_{max} .
- Under the same analysis conditions, the multi-cell bumper beam absorbed more energy than the single-cell bumper beam. For this reason, multi-cell bumper beam should definitely be preferred.

REFERENCES

1. Wenlong, S., Xiaokai, C., ve Lu, W., "Analysis of energy saving and emission reduction of vehicles using light weight materials", *Energy Procedia*, 88: 889–893 (2016).
2. Goetz, J. ve Rexhepi, M., "Modeling of Front Bumper system with emphasis on lightweight and low cost A product development project at Volvo Cars", 84 (2018).
3. Jie, X., Ping, X., Shuguang, Y., Hui, Z., Ziliang, Z., ve Zhangjun, W., "A novel weighted graph representation-based method for structural topology optimization", *Advances In Engineering Software*, 153 (July 2020): 102977 (2021).
4. Munk, D. J., Verstraete, D., ve Vio, G. A., "Effect of fluid-thermal-structural interactions on the topology optimization of a hypersonic transport aircraft wing", *Journal Of Fluids And Structures*, 75: 45–76 (2017).
5. Zhu, J. H., Gu, X. J., Zhang, W. H., ve Beckers, P., "Structural design of aircraft skin stretch-forming die using topology optimization", *Journal Of Computational And Applied Mathematics*, 246: 278–288 (2013).
6. Jankovics, D. ve Barari, A., "Customization of Automotive Structural Components using Additive Manufacturing and Topology Optimization", *IFAC-PapersOnLine*, 52 (10): 212–217 (2019).
7. Böckin, D. ve Tillman, A. M., "Environmental assessment of additive manufacturing in the automotive industry", *Journal Of Cleaner Production*, 226: 977–987 (2019).
8. Abdullah, N. A. Z., Sani, M. S. M., Salwani, M. S., ve Husain, N. A., "A review on crashworthiness studies of crash box structure", *Thin-Walled Structures*, 153 (April): 106795 (2020).
9. Hosseinipour, S. J. ve Daneshi, G. H., "Energy absorbtion and mean crushing load of thin-walled grooved tubes under axial compression", *Thin-Walled Structures*, 41 (1): 31–46 (2003).
10. González Palencia, J. C., Furubayashi, T., ve Nakata, T., "Energy use and CO2 emissions reduction potential in passenger car fleet using zero emission vehicles and lightweight materials", *Energy*, 48 (1): 548–565 (2012).
11. Okorugba, P. A., "Effect of Impact Velocity on the Energy Absorption Characteristics of Crash Boxes", *Near East University*, (2019).

12. Peroni, L., Avalle, M., ve Belingardi, G., "Comparison of the energy absorption capability of crash boxes assembled by spot-weld and continuous joining techniques", *International Journal Of Impact Engineering*, 36 (3): 498–511 (2009).
13. Xiao, Z., Fang, J., Sun, G., ve Li, Q., "Crashworthiness design for functionally graded foam-filled bumper beam", *Advances In Engineering Software*, 85: 81–95 (2015).
14. Farkas, L., Moens, D., Donders, S., ve Vandepitte, D., "Optimisation study of a vehicle bumper subsystem with fuzzy parameters", *Mechanical Systems And Signal Processing*, 32: 59–68 (2012).
15. Segade, A., Bolaño, A., López-Campos, J. A., Casarejos, E., Fernandez, J. R., ve Vilán, J. A., "Study of a crash box design optimized for a uniform load profile", (2018).
16. Eyvazian, A., Mozafari, H., ve Hamouda, A. M., "Experimental Study of Corrugated Metal-composite Tubes under Axial Loading", *Procedia Engineering*, 173: 1314–1321 (2017).
17. Wang, C. Y., Wang, W. W., Zhao, W. Z., Wang, Y., ve Zhou, G., "Structure design and multi-objective optimization of a novel NPR bumper system", *Composites Part B: Engineering*, 153 (June): 78–96 (2018).
18. Grima, J. N., Gatt, R., Alderson, A., ve Evans, K. E., "An alternative explanation for the negative Poisson's ratios in α -cristobalite", *Materials Science And Engineering: A*, 423 (1–2): 219–224 (2006).
19. Yang, S. ve Qi, C., "Multiobjective optimization for empty and foam-filled square columns under oblique impact loading", *International Journal Of Impact Engineering*, 54: 177–191 (2013).
20. Zahran, M. S., Xue, P., Esa, M. S., ve Abdelwahab, M. M., "A novel tailor-made technique for enhancing the crashworthiness by multi-stage tubular square tubes", *Thin-Walled Structures*, 122 (March 2017): 64–82 (2018).
21. Liu, W., Huang, J., Deng, X., Lin, Z., ve Zhang, L., "Crashworthiness analysis of cylindrical tubes filled with conventional and negative Poisson's ratio foams", *Thin-Walled Structures*, 131 (March 2017): 297–308 (2018).
22. Altin, M., Acar, E., ve Güler, M. A., "Foam filling options for crashworthiness optimization of thin-walled multi-tubular circular columns", *Thin-Walled Structures*, 131 (May): 309–323 (2018).
23. Wang, J., Zhang, Y., He, N., ve Wang, C. H., "Crashworthiness behavior of Koch fractal structures", *Materials And Design*, 144: 229–244 (2018).
24. Li, Z., Ma, W., Hou, L., Xu, P., ve Yao, S., "Crashworthiness analysis of corrugations reinforced multi-cell square tubes", *Thin-Walled Structures*, 150 (March): 106708 (2020).

25. Kurtuluş, E. ve Tekin, G., "Conversion of Aluminum Front Bumper System to Magnesium Material by Using Design of Experiment Method", *International Journal Of Automotive Science And Technology*, 5 (1): 34–42 (2021).
26. Li, Z., Yu, Q., Zhao, X., Yu, M., Shi, P., ve Yan, C., "Crashworthiness and lightweight optimization to applied multiple materials and foam-filled front end structure of auto-body", *Advances In Mechanical Engineering*, 9 (8): 1–21 (2017).
27. Fuchs, E. R. H., Field, F. R., Roth, R., ve Kirchain, R. E., "Strategic materials selection in the automobile body: Economic opportunities for polymer composite design", *Composites Science And Technology*, 68 (9): 1989–2002 (2008).
28. Boria, S., "Lightweight design and crash analysis of composites", *Lightweight Composite Structures in Transport*, Woodhead Publishing, 329–360 (2016).
29. Sampath Rao, P., "Design Analysis of Bumper Beam Subjected To Offset Impact Loading for Automotive Applications", *International Journal Of Mechanical Engineering And Technology*, 6 (5): 976–6340 (2015).
30. Reyes, A. ve Børvik, T., "Quasi-static behaviour of crash components with steel skins and polymer foam cores", *Materials Today Communications*, 17 (June): 541–553 (2018).
31. Gronostajski, Z., Kaczyński, P., Polak, S., ve Bartczak, B., "Energy absorption of thin-walled profiles made of AZ31 magnesium alloy", *Thin-Walled Structures*, 122 (November 2017): 491–500 (2018).
32. Dirgantara, T., Jusuf, A., Kurniati, E. O., Gunawan, L., ve Putra, I. S., "Crashworthiness analysis of foam-filled square column considering strain rate effect of the foam", *Thin-Walled Structures*, 129 (November 2017): 365–380 (2018).
33. Miyoshi, T., Itoh, M., Akiyama, S., ve Kitahara, A., "Aluminum foam, "ALPORAS": the production process, properties and applications", *Materials Research Society Symposium - Proceedings*, 521: 133–137 (1998).
34. Tanlak, N., Sonmez, F. O., ve Senaltun, M., "Shape optimization of bumper beams under high-velocity impact loads", *Engineering Structures*, 95: 49–60 (2015).
35. Tran, T., Hou, S., Han, X., Nguyen, N., ve Chau, M., "Theoretical prediction and crashworthiness optimization of multi-cell square tubes under oblique impact loading", *International Journal Of Mechanical Sciences*, 89: 177–193 (2014).
36. Qiu, N., Gao, Y., Fang, J., Feng, Z., Sun, G., ve Li, Q., "Theoretical prediction and optimization of multi-cell hexagonal tubes under axial crashing", *Thin-Walled Structures*, 102: 111–121 (2016).

37. Paz, J., Díaz, J., ve Romera, L., "Analytical and numerical crashworthiness uncertainty quantification of metallic thin-walled energy absorbers", *Thin-Walled Structures*, 157 (August): 107022 (2020).
38. Acar, E., Altin, M., ve Güler, M. A., "Evaluation of various multi-cell design concepts for crashworthiness design of thin-walled aluminum tubes", *Thin-Walled Structures*, 142 (April): 227–235 (2019).
39. Magliaro, J. ve Altenhof, W., "Analytical predictions of the complete mechanical response of AA6061 energy absorbers subjected to axial cutting", *Thin-Walled Structures*, 139 (January): 151–168 (2019).
40. Lu, Q., Qi, D., Li, Y., Xiao, D., ve Wu, W., "Impact energy absorption performances of ordinary and hierarchical chiral structures", *Thin-Walled Structures*, 140 (April): 495–505 (2019).
41. Chen, T., Zhang, Y., Lin, J., ve Lu, Y., "Theoretical analysis and crashworthiness optimization of hybrid multi-cell structures", *Thin-Walled Structures*, 142 (October 2018): 116–131 (2019).
42. Pirmohammad, S. ve Esmaeili-Marzdashti, S., "Multi-objective crashworthiness optimization of square and octagonal bitubal structures including different hole shapes", *Thin-Walled Structures*, 139 (October 2018): 126–138 (2019).
43. Li, Z., Yao, S., Ma, W., Xu, P., ve Che, Q., "Energy-absorption characteristics of a circumferentially corrugated square tube with a cosine profile", *Thin-Walled Structures*, 135 (October 2018): 385–399 (2019).
44. Xu, F., Zhang, S., Wu, K., ve Dong, Z., "Multi-response optimization design of tailor-welded blank (TWB) thin-walled structures using Taguchi-based gray relational analysis", *Thin-Walled Structures*, 131 (June): 286–296 (2018).
45. Liu, W., Lin, Z., He, J., Wang, N., ve Deng, X., "Crushing behavior and multi-objective optimization on the crashworthiness of sandwich structure with star-shaped tube in the center", *Thin-Walled Structures*, 108: 205–214 (2016).
46. Tarlochan, F., Samer, F., Hamouda, A. M. S., Ramesh, S., ve Khalid, K., "Design of thin wall structures for energy absorption applications: Enhancement of crashworthiness due to axial and oblique impact forces", *Thin-Walled Structures*, 71: 7–17 (2013).
47. Xu, X., Zhang, Y., Wang, J., Jiang, F., ve Wang, C. H., "Crashworthiness design of novel hierarchical hexagonal columns", *Composite Structures*, 194 (March): 36–48 (2018).
48. Nikkhah, H., Baroutaji, A., ve Olabi, A. G., "Crashworthiness design and optimisation of windowed tubes under axial impact loading", *Thin-Walled Structures*, 142 (December 2018): 132–148 (2019).
49. Yao, S., Huo, Y., Yan, K., ve Xu, P., "Crashworthiness study on circular hybrid

- corrugated tubes under axial impacts", *Thin-Walled Structures*, 145 (January): 106358 (2019).
50. Günay, M., Korkmaz, M. E., ve Yaşar, N., "Finite element modeling of tool stresses on ceramic tools in hard turning", *Mechanika*, 23 (3): 432–440 (2017).
 51. Korkmaz, M. E. ve Günay, M., "Finite Element Modelling of Cutting Forces and Power Consumption in Turning of AISI 420 Martensitic Stainless Steel", *Arabian Journal For Science And Engineering*, 43 (9): 4863–4870 (2018).
 52. Korkmaz, M. E., "Verification of Johnson-Cook parameters of ferritic stainless steel by drilling process: Experimental and finite element simulations", *Journal Of Materials Research And Technology*, 9 (3): 6322–6330 (2020).
 53. Liang, L., Liu, M., Elefteriades, J., ve Sun, W., "PyTorch-FEA: Autograd-enabled finite element analysis methods with applications for biomechanical analysis of human aorta", *Computer Methods And Programs In Biomedicine*, 238: (2023).
 54. Cook, R. D., "Finite Element Modeling for Stress Analysis", 1st. Baskı, *John Wiley & Sons, Inc.*, USA, (1994).
 55. Liu, Q., Li, J., ve Liu, J., "ParaView visualization of Abaqus output on the mechanical deformation of complex microstructures", *Computers And Geosciences*, 99 (June 2016): 135–144 (2017).
 56. Günay, M., Meral, T., ve Korkmaz, M. E., "Drillability Analysis of AISI 420 Martensitic Stainless Steel by Finite Element Method", *Gazi Journal Of Engineering Sciences*, 4 (3): 223–229 (2018).
 57. KORKMAZ, M. E. ve GÜNAY, M., "Confirmation of Johnson-Cook Model Parameters for Nimonic 80A alloy by Finite Element Method", *Politeknik Dergisi*, 23 (3): 625–632 (2020).
 58. Korkmaz, M. E. ve Gupta, M. K., "A State of the Art on Simulation and Modelling Methods in Machining: Future Prospects and Challenges", *Archives Of Computational Methods In Engineering*, 30 (1): 161–189 (2023).
 59. Tran, T., Hou, S., Han, X., Tan, W., ve Nguyen, N., "Theoretical prediction and crashworthiness optimization of multi-cell triangular tubes", *Thin-Walled Structures*, 82: 183–195 (2014).
 60. Li, Z., Rakheja, S., ve Shangguan, W. Bin, "Study on crushing behaviors of foam-filled thin-walled square tubes with different types and number of initiators under multiple angle loads", *Thin-Walled Structures*, 145 (September): 106376 (2019).
 61. Fang, J., Sun, G., Qiu, N., Kim, N. H., ve Li, Q., "On design optimization for structural crashworthiness and its state of the art", *Structural And Multidisciplinary Optimization*, 55 (3): 1091–1119 (2017).

62. Altin, M., Güler, M. A., ve Mert, S. K., "The effect of percent foam fill ratio on the energy absorption capacity of axially compressed thin-walled multi-cell square and circular tubes", *International Journal Of Mechanical Sciences*, 131–132 (May): 368–379 (2017).
63. Priem, C., Othman, R., Rozycki, P., ve Guillon, D., "Experimental investigation of the crash energy absorption of 2.5D-braided thermoplastic composite tubes", *Composite Structures*, 116 (1): 814–826 (2014).
64. Zarei, H., Kröger, M., ve Albertsen, H., "An experimental and numerical crashworthiness investigation of thermoplastic composite crash boxes", *Composite Structures*, 85 (3): 245–257 (2008).
65. Kathiresan, M., Manisekar, K., ve Manikandan, V., "Crashworthiness analysis of glass fibre/epoxy laminated thin walled composite conical frusta under axial compression", *Composite Structures*, 108 (1): 584–599 (2014).
66. Jiang, H., Ren, Y., ve Gao, B., "Research on the progressive damage model and trigger geometry of composite waved beam to improve crashworthiness", *Thin-Walled Structures*, 119 (January): 531–543 (2017).
67. Cherniaev, A., Butcher, C., ve Montesano, J., "Predicting the axial crush response of CFRP tubes using three damage-based constitutive models", *Thin-Walled Structures*, 129 (February): 349–364 (2018).
68. Goyal, S., Anand, C. S., Sharma, S. K., ve Sharma, R. C., "Crashworthiness analysis of foam filled star shape polygon of thin-walled structure", *Thin-Walled Structures*, 144 (January): (2019).
69. Nasution, A. Y., Rejab, M. R. M., Ma, Q., ve Firmansyah, M. A., "Design optimization of passenger SUV's crash box and bumper beam by using finite element method", *IOP Conference Series: Materials Science And Engineering*, 1068 (1): 012023 (2021).
70. Kulkarni, A., Vora, R., ve Ravi, K., "Study design and analysis of automobile bumper for pedestrian safety", *IOP Conference Series: Materials Science And Engineering*, 263 (6): (2017).
71. Mao, X., Yi, Y., Huang, S., ve He, H., "Bulging limit of AZ31B magnesium alloy tubes in hydroforming with internal and external pressure", *International Journal Of Advanced Manufacturing Technology*, 101 (9–12): 2509–2517 (2019).
72. Fridlyander, I. N., Sister, V. G., Grushko, O. E., Berstenev, V. V., Sheveleva, L. M., ve Ivanova, L. A., "Aluminum alloys: Promising materials in the automotive industry", *Metal Science And Heat Treatment*, 44 (9–10): 365–370 (2002).
73. Gao, Y., Wang, B., Chen, J., Sun, Z., ve Zhang, H., "Optimizing joint structure and performance in friction spot joining of aluminum alloy AA6061 and poly-ether-ether-ketone (PEEK)", *CIRP Journal Of Manufacturing Science And*

Technology, 47 (November): 273–282 (2023).

74. Wang, Z., Guines, D., Chu, X., ve Leotoing, L., "Prediction and characterization of forming limits at necking from shear to equi-biaxial loading using the biaxial tensile testing method: Feasibility study and application to AA6061-T4", *Mechanics Of Materials*, 179 (February): 104598 (2023).
75. Patil, R. V., Lande, P. R., Tadamalle, A. P., ve Reddy, Y. P., "Determination of Impact Absorbing Capacity and toughness of Aluminum Honeycomb Sandwich Panel in Bumper Beam", *Materials Today: Proceedings*, 4 (8): 8816–8826 (2017).
76. Sather, E., "An Analytical Method to Calculate Effective Elastic Properties of General Multifunctional Honeycomb Cores in Sandwich Composites An Analytical Method to Calculate Effective Elastic Properties of General Multifunctional Honeycomb Cores in Sandwich Composit", (April): (2019).
77. Zhang, X. G., Jiang, W., Zhang, Y., Luo, C., Zhang, X. Y., Han, D., Hao, J., Teng, X. C., Xie, Y. M., ve Ren, X., "Energy absorption properties of composite tubes with hexagonal and re-entrant honeycomb fillers", *Construction And Building Materials*, 356 (June): 129298 (2022).
78. Peng, X., Liu, G., Li, J., Wu, H., Jia, W., ve Jiang, S., "Compression property and energy absorption capacity of 4D-printed deformable honeycomb structure", *Composite Structures*, 325 (May): 117591 (2023).
79. Lu, Q. ve Deng, X., "Energy absorption and in-plane mechanical behavior of honeycomb structures with reinforced strut", *Composite Structures*, 322 (June): (2023).
80. Mohammadi, H., Ahmad, Z., Petru, M., Mazlan, S. A., Faizal Johari, M. A., Hatami, H., ve Rahimian Kolor, S. S., "An insight from nature: Honeycomb pattern in advanced structural design for impact energy absorption", *Journal Of Materials Research And Technology*, 22: 2862–2887 (2023).
81. Paz, J., Díaz, J., Romera, L., ve Costas, M., "Crushing analysis and multi-objective crashworthiness optimization of GFRP honeycomb-filled energy absorption devices", *Finite Elements In Analysis And Design*, 91: 30–39 (2014).
82. Duan, Y., Zhang, T., Zhou, J., Xiao, H., Chen, X., Al Teneiji, M., Guan, Z. W., ve Cantwell, W. J., "Energy-absorbing characteristics of hollow-cylindrical hierarchical honeycomb composite tubes inspired a beetle forewing", *Composite Structures*, 278 (August): 114637 (2021).
83. Nian, Y., Wan, S., Li, M., ve Su, Q., "Crashworthiness design of self-similar graded honeycomb-filled composite circular structures", *Construction And Building Materials*, 233: (2020).
84. Liu, H., Chen, L., Cao, J., Chen, L., Du, B., Guo, Y., Li, W., ve Fang, D., "Axial compression deformability and energy absorption of hierarchical thermoplastic

composite honeycomb graded structures", *Composite Structures*, 254 (June): 112851 (2020).

85. Liu, Q., Fu, J., Wang, J., Ma, J., Chen, H., Li, Q., ve Hui, D., "Axial and lateral crushing responses of aluminum honeycombs filled with EPP foam", *Composites Part B: Engineering*, 130: 236–247 (2017).
86. Sun, G., Chen, D., Zhu, G., ve Li, Q., "Lightweight hybrid materials and structures for energy absorption: A state-of-the-art review and outlook", *Thin-Walled Structures*, 172: 108760 (2022).

RESUME

Gökhan KAYA finished his undergraduate bachelor's program at Karabük University, Department of Mechanical Engineering in 2015. Then in 2020, he started his master's program at Karabuk University, Department of Mechanical Engineering. He is currently working at OTOKAR Automotive and Defence Industry as commercial vehicles trim systems design manager.